JACS
JOURNAL OF THE AMERICAN CHEMICAL SOCIETY
Article
pubs.acs.org/JACS

The Nature of Secondary Interactions at Electrophilic Metal Sites of Molecular and Silica-Supported Organolutetium Complexes from Solid-State NMR Spectroscopy

Matthew P. Conley,[†] Giuseppe Lapadula,[†] Kevin Sanders,[‡] David Gajan,[‡] Anne Lesage,[‡] Iker del Rosal,[§] Laurent Maron,[§] Wayne W. Lukens,[∥] Christophe Copéret,*[,†] and Richard A. Andersen*[,⊥]

[†]Department of Chemistry and Applied Biosciences, ETH Zürich, Vladimir Prelog Weg 1-5, CH-8093 Zürich, Switzerland
[‡]Centre de RMN à Très Hauts Champs, CRNS/ENS-Lyon/UCB Lyon 1, Université de Lyon, 5 rue de la Doua, 69100 Villeurbanne, France
[§]Université de Toulouse and CNRS, LPCNO INSA/UPS/CNRS, 135 avenue de Rangueil, 31077 Toulouse Cedex 4, France
[∥]Chemical Sciences Division, Lawrence Berkeley National Laboratory, Berkeley, California 94720, United States
[⊥]Department of Chemistry, University of California, Berkeley, California 94720, United States

Supporting Information

ABSTRACT: $Lu[CH(SiMe_3)_2]_3$ reacts with $[SiO_{2-700}]$ to give $[(\equiv SiO)Lu[CH(SiMe_3)_2]_2]$ and $CH_2(SiMe_3)_2$. $[(\equiv SiO)Lu[CH(SiMe_3)_2]_2]$ is characterized by solid-state NMR and EXAFS spectroscopy, which show that secondary Lu···C and Lu···O interactions, involving a γ-CH_3 and a siloxane bridge, are present. From X-ray crystallographic analysis, the molecular analogues $Lu[CH(SiMe_3)_2]_{3-x}[O\text{-}2,6\text{-}t\text{Bu-}C_6H_3]_x$ (x = 0−2) also have secondary Lu···C interactions. The ^{1}H NMR spectrum of $Lu[CH(SiMe_3)_2]_3$ shows that the $-SiMe_3$ groups are equivalent to −125 °C and inequivalent below that temperature, $\Delta G^{\ddagger}_{(T_c\,=\,148\ K)}$ = 7.1 kcal mol^{-1}. Both $-SiMe_3$ groups in $Lu[CH(SiMe_3)_2]_3$ have $^1J_{CH}$ = 117 ± 1 Hz at −140 °C. The solid-state ^{13}C CPMAS NMR spectrum at 20 °C shows three chemically inequivalent resonances in the area ratio of 4:1:1 (12:3:3); the J-resolved spectra for each resonance give $^1J_{CH}$ = 117 ± 2 Hz. The ^{29}Si CPMAS NMR spectrum shows two chemically inequivalent resonances with different values of chemical shift anisotropy. Similar observations are obtained for $Lu[CH(SiMe_3)_2]_{3-x}[O\text{-}2,6\text{-}t\text{Bu-}C_6H_3]_x$ (x = 1 and 2). The spectroscopic data point to short Lu···Cγ contacts corresponding to 3c-2e Lu···Cγ−Siβ interactions, which are supported by DFT calculations. Calculated natural bond orbital (NBO) charges show that Cγ carries a negative charge, while Lu, Hγ, and Siβ carry positive charges; as the number of O-based ligands increases so does the positive charge at Lu, which in turns shortens the Lu···Cγ distance. The change in NBO charges and the resulting changes in the spectroscopic and crystallographic properties show how ligands and surface-support sites rearrange to accommodate these changes, consistent with Pauling's electroneutrality concept.

Si_β-C_γ polarization modulated by Electrophilic Metal Sites

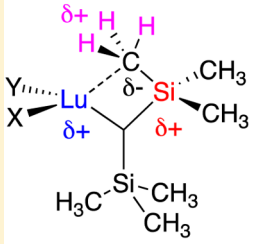

Highlighted by
^{13}C and ^{29}Si solid-state NMR
DFT Calculations
X-ray Adsorption and Diffraction

δ+ at Lu: X = Y = Alkyl < X = Alkyl, Y= OR < Y = X = OR

INTRODUCTION

Secondary interactions between a metal and its carbyl ligands are often postulated to play an important role in stabilizing ground states and transition states in catalytic reactions. The interaction implies that electrons in a specific bond in a ligand are in close contact with the electrophilic metal site. These secondary interactions are often encountered in 3-center-2-electron (3c-2e) bond interactions between an empty orbital on the metal with the pair of electrons in a σ-C−H bond and are labeled agostic C−H interactions (Figure 1a).[1−3] The presence of α-, β-, and/or γ-C−H agostic interactions is often postulated in the transition states for insertion of olefins.[4−7] For example, the α-CH agostic interaction found in the transition state in metal-catalyzed polymerization of polypropylene is thought to direct the stereoselectivity in the polymer products.[5,6] The insertion of an olefin into an early metal−alkyl bond can generate a γ-CH agostic interaction, which are proposed intermediates in metal-catalyzed olefin polymerization reactions.[1,3] β-C−H Agostic interactions are intermediates in late transition-metal olefin polymerization catalysts that undergo chain-walking to form hyper-branched polyolefins.[7] The agostic interaction is also an important component in stabilizing the *syn*-configuration of Schrock-type alkylidene complexes, essential for the stereoselective production of alkenes in metathesis reactions.[8−14] This brief outline illustrates that

Received: January 4, 2016
Published: February 18, 2016

DOI: 10.1021/jacs.6b00071
J. Am. Chem. Soc. 2016, 138, 3831−3843

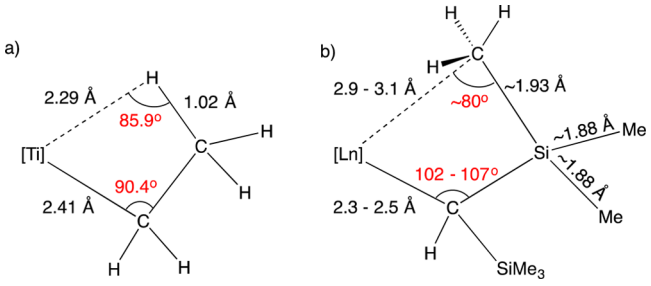

Figure 1. Structural features of (a) the β-CH agostic interaction in (dmpe)Ti(Et)Cl_3 and (b) the secondary interactions in Ln[CH-$(SiMe_3)_2]_3$.

agostic interactions are conceptually important in many metal-catalyzed reactions.[15,16]

Several structural features are characteristic of ground-state β-C−H agostic interactions in d-block transition metals. In general, the C−H bond is elongated, the M···HC is shortened, and the M···CC angles become more acute than expected for a sp^3-hybridized carbon in the absence of such an interaction.[3] One of the first structurally characterized complexes containing an agostic interaction was (dmpe)Ti(Et)Cl_3 (dmpe =1,2-bis(dimethylphosphino)ethane), in which the bond distances and angles are summarized in Figures 1a.[17,18] α-C−H Agostic interactions are also observed in d^0 alkylidene metathesis catalysts documented by acute M−C−H bond angles.[8,11,12,19,20] In addition to bond distance and angle changes, several spectroscopic observables have been used to support the presence of agostic interactions: the ^{1}H NMR chemical shift in the diamagnetic compound of the H atom involved in an agostic interaction shifts upfield from the free alkane, and the $^1J_{CH}$ becomes substantially lower than ca. 125 Hz in sp^3 C−H bonds.[3,11,21,22] The low coordinate tris-bis(trimethylsilyl)-methyl lanthanide complexes, Ln[$CH(SiMe_3)_3]_3$, with Ln = Y,[23] La,[24] Ce,[23] and Sm,[24] contain unusually short distances between the metal and one $-SiMe_3$ group of the pendant alkyl in their X-ray crystal structures. The distortion of a CH-$(SiMe_3)_2$ group is also a general pattern observed in the crystal structures of Cp^*_{3-x}Ln[$CH(SiMe_3)_2]_x$, where x = 1 or 2.[25−33] Regardless of the reasons, these secondary interactions are a signature of the electrophilicity of the lanthanide in these compounds.

In view of our long-standing interest in understanding the influence of a surface siloxy group on the reactivity of well-defined supported catalysts,[34−38] we became interested in using secondary interactions in Ln[$CH(SiMe_3)_3]_3$ as a way to evaluate the electrophilicity in silica-supported (≡Si)OLn-[$CH(SiMe_3)_2]_2$. Here we describe the nature of metal-hydrocarbyl ligand secondary interactions in organolutetium silica-supported surface species (≡SiO)Lu[$CH(SiMe_3)_2]_2$ and its corresponding molecular analogues Lu[$CH(SiMe_3)_2]_x$[O-2,6-$tBu_2C_6H_3]_{3-x}$, x = 0−2. The monomeric, three coordinate molecules have short Lu···Cγ distances in their solid-state crystal structures, the nature of which is defined by solution- and solid-state NMR spectroscopies as a 3c-2e Ln···CγSiγ interaction, better described as an asymmetric bridging methyl between Lu and Si than an agostic Lu···H−Cγ. This experimental deduction is supported by DFT calculations and in particular natural bond orbital (NBO) charges that depend on the alkyl/alkoxide ratio. The model developed from the molecular compounds is used to rationalize the structure of the supported species (≡SiO)Lu[$CH(SiMe_3)_2]_2$, obtained by EXAFS spectroscopy. The combination of solution- and solid-state spectroscopic studies, supported by the calculation of the NBO charges, provides a detailed understanding of the intramolecular interactions in these molecular and silica-supported organometallic compounds and documents the role of O-based ligands in tuning the electrophilicity of the lutetium center.

EXPERIMENTAL SECTION

General Considerations. All the experiments were carried under dry, oxygen-free argon using Schlenk and glovebox techniques. For preparation of surface species, reactions were carried out using high-vacuum lines (10^{-5} mbar) and glovebox techniques. Pentane was purified using a double MBraun SPS alumina column, degassed before use, and stored over 4 Å molecular sieves or by distillation from sodium. Benzene was distilled from purple Na/benzophenone. Deuterated solvents were degassed by three freeze−pump−thaw cycles and distilled from Na/benzophenone by vacuum transfer into flame sealable NMR tubes. Lu$(N(SiMe_3)_2)_3$ was synthesized by a modified literature procedure using Lu$(OTf)_3$ and $NaN(SiMe_3)_2$ in Et_2O; the crude solid was sublimed, and the sublimate was crystallized from pentane.[39] Lu[O-2,6-$(Me_3C)_2C_6H_3]_3$ was prepared by the reaction of Lu$(N(SiMe_3)_2)_3$ and sublimed 2,6-di-t-butylphenol as described in the literature.[40] Silica (Sylapol-948 ca. 900 m^2/g) was partially dehydroxylated according a published procedure[41] and contains 0.35 mmol SiOH g^{-1}. All infrared (IR) spectra were recorded using a Bruker α spectrometer located in an Ar-filled glovebox equipped with OPUS software; typically 32 scans were accumulated for each spectrum. Elemental analysis was performed at Mikroanalytisches Laboratorium Pascher, Germany.

Solution ^{1}H, ^{13}C, and ^{29}Si NMR spectra were obtained using a Bruker DRX 400 spectrometer at room temperature. The ^{1}H, ^{13}C, and ^{29}Si chemical shifts were referenced relative to the residual solvent peaks and reported relative to $SiMe_4$. The solid-state magic angle spinning (MAS) NMR spectra were recorded on Bruker Avance III spectrometers operating at 500, 700, or 800 MHz (see figure captions). Samples were loaded into 3.2 or 4 mm zirconia rotors in the glovebox and sealed with PTFE caps. ^{1}H, ^{13}C, and ^{29}Si chemical shifts were referenced to external TMS. The two-dimensional (2D) J-resolved experiments were performed as previously described:[42] after cross-polarization (CP) from protons, carbon magnetization evolved during t_1 under proton homonuclear decoupling. Simultaneous 180° carbon and proton pulses were applied in the middle of t_1 to refocus the carbon chemical shift evolution while retaining the modulation by the heteronuclear J_{CH} scalar couplings. A Z-filter was finally applied to allow phase-sensitive detection in ω_1. Proton homonuclear decoupling was performed by using the eDUMBO sequence.[43] The proton radio frequency (RF) field strength was set to 100 kHz during t_1 (eDUMBO decoupling) and acquisition (SPINAL-64 decoupling).[44] For each J-resolved spectrum recorded on the molecular complexes, the scaling factor was carefully evaluated from an experiment recorded on L-alanine with the exact same parameter set. The observed J-quadruplet of the CH_3 group was fitted, and the extracted scaled J coupling value was compared with that measured in solution (130 Hz). The 2D proton carbon-13 correlation specrta were aquired using a conventional heteronuclear correlation (HETCOR) experiment, which consists first in a 90° proton pulse, followed by a t_1 evolution period under proton isotropic chemical shift, and a CP step to transfer magnetization on the neighboring carbon-13 spins. SPINAL-64 heteronuclear decoupling (during t_2) and e-DUMBO-22 homonuclear decoupling (during t_1) were applied at RF fields of 100 kHz. Quadrature detection in ω_1 was achieved using the TPPI method for both type of experiments.[45]

EXAFS Spectroscopy. Samples were loaded into an aluminum holder equipped with aluminized Mylar windows sealed with an indium gasket in an Ar-filled inert atmosphere glovebox. Assembled holders were sealed in glass jars until just prior to data collection. At the beamline, the jar was opened, and the sample was quickly transferred to a helium-filled cryostat, which was evacuated then

DOI: 10.1021/jacs.6b00071
J. Am. Chem. Soc. 2016, 138, 3831−3843

refilled with helium gas three times. Data were obtained at room temperature (the cryostat was only used to provide additional oxygen protection). X-ray absorption data were obtained at beamline 4-1 of Stanford Synchrotron Radiation Lightsource. The X-ray beam was monochromatized using a double crystal monochromator with Si(220), ϕ = 90° crystals. The second crystal was detuned by 50% to reduce the harmonic content of the beam. Data were obtained in transmission at the lanthanide L_3-edge using N_2-filled ion chambers. Data were deglitched using the EXAFSPAK suite of programs written by Graham George. Data were treated to remove the pre- and postedge backgrounds, and the EXAFS were obtained by subtracting a spline from the absorption data using the software package Athena.[46,47] EXAFS data were fit using the software package Artemis using theoretical scattering curves generated by Feff7.[48]

All DFT calculations were performed with Gaussian 09.[49] Calculations were carried out at the DFT level of theory using the hybrid functional B3PW91.[50−54] Geometry optimizations were achieved without any symmetry restriction. Calculations of vibrational frequencies were systematically done in order to characterize the nature of stationary points. Stuttgart effective core potentials[55,56] and their associated basis set augmented with a polarization function (ζf = 1.0) were used for lutetium. Carbon and oxygen atoms were treated with 6-31G(d,p) double-ζ basis sets,[57,58] whereas silicon and hydrogen atoms were treated with Dunning's cc-pVTZ basis set.[59] Among the various theories available to compute chemical shielding tensors, the gauge including atomic orbital (GIAO) method was adopted for the numerous advantages it presents.[60−63] The electron density and partial charge distribution were examined in terms of localized electron-pair bonding units using the NBO program.[64,65] Through this method, the input atomic orbital basis set was transformed via natural atomic orbitals (NAOs) and natural hybrid orbitals (NHOs) into NBOs, which correspond to the localized one center ("lone pair") and two-center ("bond") elements of the Lewis structure. All the possible interactions between "filled" (donor) Lewis-type NBOs and "empty" (acceptor) non-Lewis NBOs orbitals, together with their energetic quantification (stabilization energy), were obtained by a second-order perturbation theory analysis of the Fock matrix.

Preparation of Lu[CH(SiMe$_3$)$_2$]$_3$. Lu(O-2,6-*t*Bu$_2$-C$_6$H$_3$)$_3$ (1.20 g, 1.51 mmol) was dissolved in 30 mL of pentane. A solution of Li[CH(SiMe$_3$)$_2$] (0.811 g, 4.89 mmol, 3.2 equiv)[66,67] was dissolved in a mixture of pentane (90 mL) and toluene (10 mL), and the solution was added to the solution of Lu(O-2,6-Me$_2$-C$_6$H$_3$)$_3$ at 20 °C dropwise over ca. 45 min using an addition funnel. A thick white precipitate formed. The mixture was stirred at room temperature for 16 h. The volatile materials were removed under reduced pressure, resulting in a white solid. Pentane (30 mL) was added by cannula, and the insoluble white precipitate was separated by filtration. The clear colorless pentane solution was concentrated to ca. 10 mL and cooled to −40 °C. Large clear blocky needles of the product were isolated in two crops by filtration. The needles contain 0.25 equiv of CH$_2$(SiMe$_3$)$_2$ as deduced by the solution ^{1}H NMR spectrum; yield 0.403 g (41%). Dissolving the solid in toluene, removing the solvent at high vacuum (10^{-5} mbar), and repeating this treatment seven times yields Lu[CH(SiMe$_3$)$_2$]$_3$·0.39 PhCH$_3$·0.03 CH$_2$(SiMe$_3$)$_2$ according to solution ^{1}H NMR spectroscopy. ^{1}H NMR (C$_7$D$_{14}$, 20 °C): δ 0.36 (18H, s, Lu-CH(Si*Me*$_3$)$_2$, −0.81 (1H, Lu-C*H*(SiMe$_3$)$_2$) and resonances due to toluene and (Me$_3$Si)$_2$CH$_2$; ^{13}C NMR: δ 59.8 (Lu-*C*H(SiMe$_3$)$_2$, $^1J_{CH}$ = 91 Hz), 5.6 (Lu-CH(Si*Me*$_3$)$_2$, $^1J_{CH}$ = 118 Hz). ^{29}Si{^{1}H} NMR: δ −8.7 (s). ^{13}C cross-polarization magic angle spinning (CPMAS) NMR: δ 57.7, 5.4, 4.7, 4.5; ^{29}Si CPMAS NMR: δ −11.75, −5.25. Elemental analysis: Calcd for C$_{21}$H$_{57}$Si$_6$Lu·(CH$_2$(SiMe$_3$)$_2$)$_{0.25}$: C, 39.41; H, 9.01. Found: C, 39.63; H, 8.95. EIMS (M − 15)$^+$ 637 and (M − 14)$^+$ 638.

Preparation of Lu[CH(SiMe$_3$)$_2$]$_2$[O-2,6-*t*Bu$_2$-C$_6$H$_3$]. Lu(O-2,6-*t*Bu$_2$-C$_6$H$_3$)$_3$ (0.567 g, 0.72 mmol) was dissolved in 30 mL of pentane. A solution of Li[CH(SiMe$_3$)$_2$] (0.238 g, 1.4 mmol, 2 equiv) dissolved in a mixture of pentane (70 mL) and toluene (5 mL) was added to the solution of Lu(O-2,6-*t*Bu$_2$-C$_6$H$_3$)$_3$ at 20 °C dropwise over ca. 45 min using an addition funnel. A thick white precipitate formed. The mixture was stirred at room temperature for 16 h. The volatile materials were removed under reduced pressure, resulting in a white solid. Pentane (50 mL) was added by cannula, and the insoluble white precipitate was separated by filtration. The clear colorless pentane solution was concentrated to ca. 30 mL and placed at −40 °C. Large clear blocks of the product were isolated by filtration. Yield 0.103 g (21%). ^{1}H NMR (C$_6$D$_6$): δ 7.28 (2H, d, $^3J_{HH}$ = 8 Hz), 6.86 (1H, t, $^3J_{HH}$ = 8 Hz), 1.52 (18H, s), 0.33 (36H, s, Lu-CH(Si*Me*$_3$)$_2$), −0.62 (2H, s, Lu-C*H*(SiMe$_3$)$_2$); ^{13}C NMR: δ 161.2, 137.3, 125.3, 118.3, 51.0 (Lu-*C*H(SiMe$_3$)$_2$, $^1J_{CH}$ = 92 Hz), 34.7, 32.0, 4.8 (Lu-CH(Si*Me*$_3$)$_2$, $^1J_{CH}$ = 117 Hz); ^{29}Si{^{1}H} NMR: δ −8.1 ppm. ^{13}C CPMAS NMR: δ 160.6,136.3, 135.5, 123.2,116.1, 115.5, 55.5, 47.7, 46.4, 32.9, 32.6, 30.7, 29.3, 4.6, 3.8, 3.0; ^{29}Si CPMAS NMR: δ −3.2, −4.1, −11.9, −12.8. Elemental analysis: Calcd for C$_{28}$H$_{59}$OSi$_4$Lu: C, 48.14; H, 8.45. Found: C, 48.25; H, 8.51. MP 83−85 °C (turned red), EIMS: (M − 15)$^+$ 683 and (M−14)$^+$ 684. The compound sublimed at 170−175 °C in diffusion pump vacuum.

Preparation of Lu[CH(SiMe$_3$)$_2$][O-2,6-*t*Bu$_2$-C$_6$H$_3$]$_2$. Lu(O-2,6-*t*Bu$_2$-C$_6$H$_3$)$_3$ (1.22 g, 1.54 mmol) was dissolved in 30 mL of pentane. A solution of Li[CH(SiMe$_3$)$_2$] (0.281 g, 1.70 mmol, 1.1 equiv) was dissolved in a mixture of pentane (90 mL) and toluene (5 mL), and the solution was added to the solution containing Lu(O-2,6-*t*Bu$_2$-C$_6$H$_3$)$_3$ at 20 °C dropwise over ca. 45 min using an addition funnel. A thick white precipitate formed. The mixture was stirred at room temperature for 16 h. The volatiles were removed under reduced pressure, resulting in a white solid. Pentane (50 mL) was added by cannula, and the insoluble white precipitate was separated by filtration. The clear colorless pentane solution was concentrated to ca. 15 mL and placed at 4 °C. Large clear blocks of the product were isolated by filtration in two crops. Yield 0.546 g (60%). ^{1}H NMR (C$_6$D$_6$): δ 7.24 (2H, d, $^3J_{HH}$ = 8 Hz), 6.82 (1H, t, $^3J_{HH}$ = 8 Hz), 1.53 (36H, s), 0.36 (18H, s, Lu-CHSi*Me*$_3$), 0.050 (1H, s, Lu-C*H*SiMe$_3$); ^{13}C NMR: δ 160.5, 136.9, 125.4, 118.3, 42.5 (Lu-C*H*SiMe$_3$, $^1J_{CH}$ = 96 Hz), 37.8, 31.9, 4.6 (Lu-CHSi*Me*$_3$, $^1J_{CH}$ = 116 Hz); ^{29}Si{^{1}H} NMR: δ −9.0. ^{13}C CPMAS NMR: δ 159.5, 158.2, 135.4, 134.7, 134.2, 125.3, 123.0, 122.8, 121.4, 116.6, 116.3, 42.8, 32.9, 32.6, 30.9, 30.2, 29.6, 29.3, 2.8; ^{29}Si CPMAS NMR: δ −4.6, −13.4. Elemental analysis: Calcd for C$_{35}$H$_{61}$O$_2$Si$_2$Lu: C, 56.43; H, 8.25. Found: C, 56.15; H, 8.46.

Grafting Lu(CH(SiMe$_3$)$_2$)$_3$ on [SiO$_2$$_{-700}$]. Sylapol-948 dehydroxylated at 700 °C (0.106 g, 0.10 mmol SiOH) was contacted with a C$_6$H$_6$ solution (2 mL) containing Lu(CH(SiMe$_3$)$_2$)$_3$ (0.075 g, 0.11 mmol) for 3.5 h. The solution was filtered, and the solid was washed with benzene (3 × 2 mL) and then with pentane (5 mL), and the solid was dried on a high vacuum line for 1 h. The combined benzene filtrate contained 0.10 mmol (Me$_3$Si)$_2$CH$_2$ by ^{1}H NMR relative to Cp$_2$Fe as an internal standard. ^{1}H MAS NMR: δ 0.1 (Lu-CH(*SiMe*$_3$)$_2$), −0.8 (Lu-C*H*(SiMe$_3$)$_2$); ^{13}C CPMAS NMR: δ 50 and 3 ppm; ^{29}Si CPMAS NMR: −8 and −6 ppm. Elemental analysis: 6.07% Lu, 5.94% C.

RESULTS

Synthesis of Lu[CH(SiMe$_3$)$_2$]$_{3-x}$[O-2,6-*t*Bu$_2$-C$_6$H$_3$]$_x$ (x = 0,1,2). Addition of Li[CH(SiMe$_3$)$_2$] in a mixture of pentane/toluene to the aryloxide Lu[O-2,6-*t*Bu$_2$-C$_6$H$_3$]$_3$ forms the lutetium alkyl compounds and Li[O-2,6-*t*Bu$_2$-C$_6$H$_3$] as illustrated in Scheme 1. The extent of alkylation depends on the stoichiometry of the reactants; 3 equiv affords Lu[CH(SiMe$_3$)$_2$]$_3$ and 1 or 2 equiv of Li[CH(SiMe$_3$)$_2$] affords Lu[CH(SiMe$_3$)$_2$][O-2,6-*t*Bu$_2$-C$_6$H$_3$]$_2$ or Lu[CH(SiMe$_3$)$_2$]$_2$[O-

Scheme 1. Synthesis of Lu[CH(SiMe$_3$)$_2$]$_{3-x}$[O-2,6-*t*Bu$_2$-C$_6$H$_3$]$_x$ (x = 0,1,2)

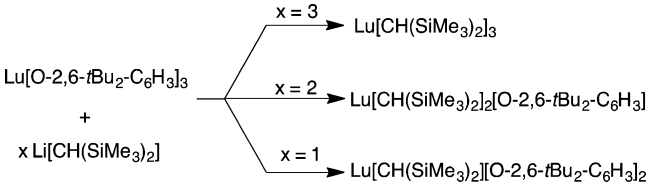

DOI: 10.1021/jacs.6b00071
J. Am. Chem. Soc. 2016, 138, 3831−3843

2,6-*t*Bu$_2$-C$_6$H$_3$], respectively. All three alkyl derivatives are isolated by crystallization from pentane as clear colorless crystals. The specific product formed is determined by the reaction stoichiometry, which implies that the individual compounds are stable to ligand redistribution reactions in hydrocarbon solution at 20 °C. Solutions of Lu[CH(SiMe$_3$)$_2$]$_2$[O-2,6-*t*Bu$_2$-C$_6$H$_3$] or Lu[CH(SiMe$_3$)$_2$][O-2,6-*t*Bu$_2$-C$_6$H$_3$]$_2$ in C$_6$D$_6$ at 20 °C are stable for over one month, indicating that this implication is correct.

Reaction of Lu[CH(SiMe$_3$)$_2$]$_3$ with Partially Dehydroxylated Silica. Contacting silica partially dehydroxylated at 700 °C (Sylapol-948, 0.35 mmol OH.g^{-1}) with benzene solutions of Lu[CH(SiMe$_3$)$_2$]$_3$ yields 1.0 equiv of CH$_2$(SiMe$_3$)$_2$ per surface silanol. The infrared spectrum of the resulting material, (≡SiO)Lu[CH(SiMe$_3$)$_2$]$_2$ (Scheme 2), lacks the ν_{OH} vibrations

Scheme 2. Reaction of Lu[CH(SiMe$_3$)$_2$]$_3$ and [SiO$_{2\text{-}700}$] To Form (≡SiO)Lu[CH(SiMe$_3$)$_2$]$_2$

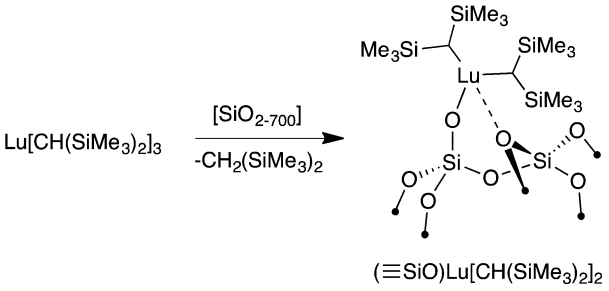

characteristic of free surface silanols, indicating that Lu[CH(SiMe$_3$)$_2$]$_3$ grafts quantitatively on the silica surface (see Supporting Information). This material contains 6.07% Lu, corresponding to 0.347 mmol g^{-1}, with 14 ± 1 C/Lu from elemental analysis that supports the stoichiometry of Scheme 2.

The solid-state ^{1}H MAS NMR spectrum of (≡SiO)Lu[CH(SiMe$_3$)$_2$]$_2$ contains two signals at −0.6 and 0.3 ppm, assigned to the α-CH and the methyl groups of −SiMe$_3$, respectively. These chemical shifts are similar to the values obtained for Lu[CH(SiMe$_3$)$_2$]$_2$[O-2,6-*t*Bu$_2$-C$_6$H$_3$] in C$_6$D$_6$ solution of −0.62 and 0.33 ppm, respectively. The ^{13}C CPMAS spectrum of (≡SiO)Lu[CH(SiMe$_3$)$_2$]$_2$ with short contact time (600 μs) contains two resonances at 50 and 3 ppm assigned to the Lu-C*H* and −Si*Me*$_3$ groups, respectively, which may be compared to the resonances at 51.0 and 4.8 ppm in Lu[CH(SiMe$_3$)$_2$]$_2$[O-2,6-*t*Bu$_2$-C$_6$H$_3$] in C$_6$D$_6$. The ^{29}Si CPMAS NMR spectrum contains two signals at −8 and −6 ppm, indicating the presence of two inequivalent silicons in (≡SiO)Lu[CH(SiMe$_3$)$_2$]$_2$; a solution of Lu[CH(SiMe$_3$)$_2$]$_2$[O-2,6-*t*Bu$_2$-C$_6$H$_3$] has a single ^{29}Si resonance at −8.1 ppm. The spectra of (≡SiO)Lu[CH(SiMe$_3$)$_2$]$_2$ are available in the Supporting Information.

The extended X-ray absorption fine structure (EXAFS) fit for the silica-supported species is shown in Figure 2, and the results of the fitting are summarized in Table 1. The short Lu−O distance (2.04 Å) is assigned to a surface siloxy group and is close to Lu−O bond distances reported for alkoxide and aryloxide complexes (2.0−2.1 Å)[68−70] and to the average Lu−O distance in Lu[CH(SiMe$_3$)$_2$]$_2$[O-2,6-*t*Bu$_2$-C$_6$H$_3$] of 2.032 ± 0.006 Å for the two independent molecules in the unit cell, see below. Two carbon atom scatters at 2.32 Å are assigned to the Lu-CH(SiMe$_3$)$_2$ carbons that are near the average value of the Lu−C bond distance obtained in the solid-state structure of Lu[CH(SiMe$_3$)$_2$]$_2$[O-2,6-*t*Bu$_2$-C$_6$H$_3$] of 2.32 ± 0.02 Å, see

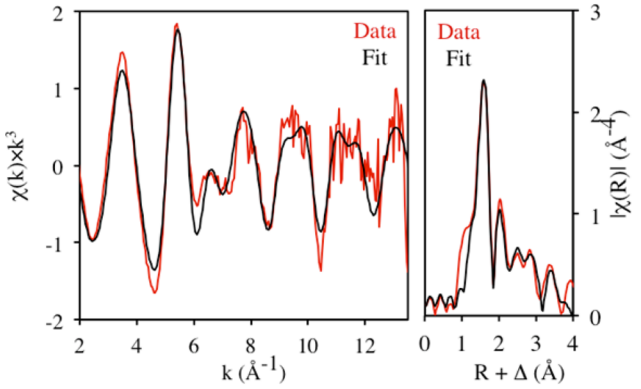

Figure 2. Lu L$_3$-edge EXAFS spectrum of (≡SiO)Lu[CH(SiMe$_3$)$_2$]$_2$.

Table 1. EXAFS Parameters for (≡SiO)Lu[CH(SiMe$_3$)$_2$]$_2$

element	no. of atoms[a]	distance (Å)	σ^2 (Å^2)	p
O	1	2.038(7)	0.0040(6)	<0.001
C	2	2.32(1)	0.011(2)	<0.001
C	1	2.80(2)	0.006(2)	0.003
O	1	3.23(2)	0.004(1)	0.002
C	1	3.87(2)	0.002(2)	0.061

[a] S_0^2 = 1 (fixed), E_0 = 7(1) eV.

below. The next scattering shell contains long-range Lu−O and Lu−C scatters at 3.23 and 3.87 Å, respectively. Interestingly, one carbon atom at 2.80 Å must be included in the fit and is attributed to a secondary Lu···Cγ interaction.[71] In the crystal structure of Lu[CH(SiMe$_3$)$_2$]$_2$[O-2,6-*t*Bu$_2$-C$_6$H$_3$] shown in Figure 3a, two Lu···Cγ distances of 2.66 ± 0.03 and 2.70 ± 0.02 Å are observed.

Solid-State Structures of Lu[CH(SiMe$_3$)$_2$]$_{3-x}$[O-2,6-*t*Bu$_2$-C$_6$H$_3$]$_x$ (x = 0,1,2). Single crystals of Lu[CH(SiMe$_3$)$_2$]$_3$, Lu[CH(SiMe$_3$)$_2$]$_2$[O-2,6-*t*Bu$_2$-C$_6$H$_3$], and Lu[CH(SiMe$_3$)$_2$][O-2,6-*t*Bu$_2$-C$_6$H$_3$]$_2$ were grown from concentrated pentane solutions, and their solid-state structures are shown in Figures 3 and 4, respectively. Selected bond distances and angles are given in Table 2, and crystal data are available in the Supporting Information.

The ORTEP of Lu[CH(SiMe$_3$)$_2$]$_3$ is shown in Figure 3a and summarized graphically in Figure 3b. As found in other Ln[CH(SiMe$_3$)$_2$]$_3$ complexes (La, Ce, and Sm),[23,24] Lu[CH(SiMe$_3$)$_2$]$_3$ crystallizes in the *P*31*c* space group. The crystal contains 0.3 equiv of disordered CH$_2$(SiMe$_3$)$_2$ in the unit cell. Lu[CH(SiMe$_3$)$_2$]$_3$ adopts a pyramidal geometry with lutetium out of the plane defined by the three carbon atoms by 0.89 Å. The Lu−C(1) distance is 2.319(3) Å, similar to those found in other Ln[CH(SiMe$_3$)$_2$]$_3$ complexes. The molecule has C_3 symmetry since the −SiMe$_3$ groups are oriented like the blades of a propeller.[23,24] The Lu···C(2) distance is 2.937(4) Å, and the Lu···Si(2) distance is 3.242(1) Å. The asymmetry in the Lu···C(2) and Lu···Siβ distances are associated with the Lu···C(1)Si(2) and Lu···C(1)Si(1) angles of 101.9(1) and 127.7(1) °, respectively. The Si−C bond lengths are often used as indicators for the presence or absence of secondary Siγ−Cγ interaction in Ln[CH(SiMe$_3$)$_2$]$_3$ compounds. In Lu[CH(SiMe$_3$)$_2$]$_3$, the Si(2)−C(2) distance is 1.907(3) Å, significantly lengthened relative to the other five Si(2)−C(3,4) and Si(1)−C(5,6,7) distances that average to 1.871 ± 0.005 Å.

The observation of asymmetry in bond lengths and angles in the lutetium alkyl-related compounds is generally ascribed to an

DOI: 10.1021/jacs.6b00071
J. Am. Chem. Soc. 2016, 138, 3831−3843

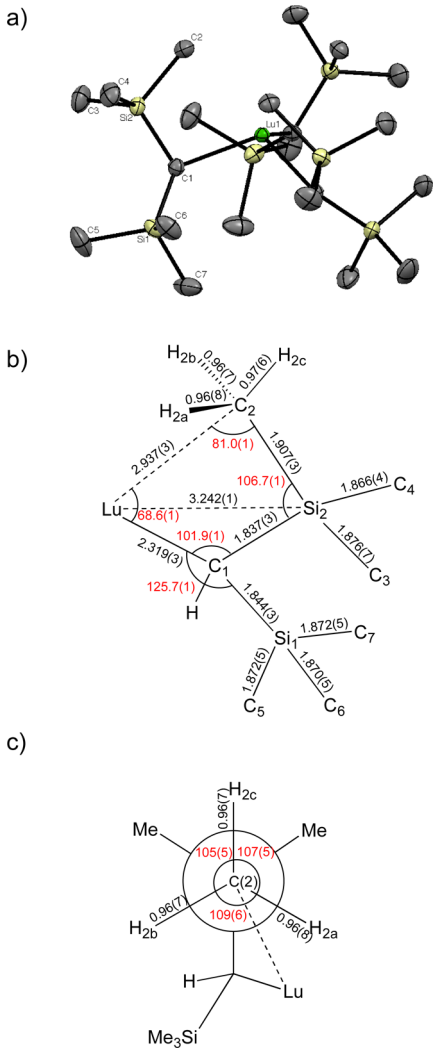

Figure 3. (a) ORTEP of $Lu[CH(SiMe_3)_2]_3$ with 50% probability ellipsoids. The heavy atoms are refined anisotropically, and the hydrogen atoms are located and refined isotropically. For clarity the hydrogen atoms and the 0.3 equiv of disordered $CH_2(SiMe_3)_2$ are omitted. Selected distances and angles are shown in Table 2; (b) sketch of relevant bond lengths (Å in black) and angles (°, red) in $Lu[CH(SiMe_3)_2]_3$; and (c) Newman projection down the C(2)−Si(2) bond with bond lengths and angles (in red) obtained from the crystal structure of $Lu[CH(SiMe_3)_2]_3$.

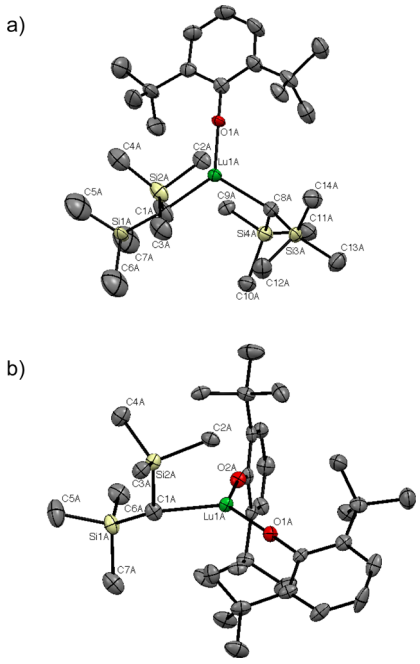

Figure 4. (a) ORTEP of a molecule in the unit cell of $Lu[CH(SiMe_3)_2]_2[O\text{-}2,6\text{-}tBu_2\text{-}C_6H_3]$; the thermal ellipsoids are at 50% probability. For clarity the hydrogen atoms are omitted. Non-hydrogen atoms are refined anisotropically, and the hydrogen atoms are placed in the calculated positions and not refined. The carbon atoms 1A and 8A are disordered. (b) ORTEP of one of the molecules in the unit cell of $Lu[CH(SiMe_3)_2][O\text{-}2,6\text{-}tBu_2\text{-}C_6H_3]_2$ at 50% probability. For clarity the hydrogen atoms are omitted. Non-hydrogen atoms are refined anisotropicall,y and the hydrogen atoms are placed in the calculated positions and not refined. Selected distances and angles are shown in Table 2.

agostic M···H−Cγ or a M···Cγ−Siβ interaction.[72] A distinction between these two descriptions can be made by analyzing the orientation of hydrogen atoms on the C(2) methyl group, that is, whether they point toward or away from the metal in the crystal structure, and the $^1J_{CH}$ values in the ^{13}C NMR spectrum. As shown in Figure 3c, the orientation of the C(2)-H(2a,b,c) bonds in $Lu[CH(SiMe_3)_2]_3$, which are located and refined isotropically, are oriented away from Lu with H−Cγ−H angles close to tetrahedral values. The Lu−C(1)−C(2)−H(2c) torsion angle is 176(7)°, while the Lu−C(1)−C(2)−H(2a) and Lu−C(1)−C(2)−H(2b) torsion angles are 66(4)° and 43(4)°, respectively. These torsion angles are inconsistent with that expected for an agostic M···H−Cγ interaction, though consistent with a 3c-2e M···Cγ−Siβ interaction as originally suggested by Morokuma.[73] A similar set of torsion angles is found in $Yb(dmpe)[N(SiMe_3)_2]_2$,[74,75] and in the neutron diffraction structure of $Cp^*La[CH(SiMe_3)_2]_2$[76] and is interpreted similarly. This contention is supported by solution and, more importantly, solid-state NMR spectra of $Lu[CH(SiMe_3)_2]_3$ described in the following section.

The ORTEP's for $Lu[CH(SiMe_3)_2]_2[O\text{-}2,6\text{-}tBu_2\text{-}C_6H_3]$ and $Lu[CH(SiMe_3)_2][O\text{-}2,6\text{-}tBu_2\text{-}C_6H_3]_2$ are shown in Figure 4a,b, respectively. Both of these molecules crystallize with two independent molecules in their unit cells, only one of which is shown in the Figure; the other ones can be found in Figures S5 and S6. One of the Lu−$CH(SiMe_3)_2$ fragments in one independent molecule of $Lu[CH(SiMe_3)_2]_2[O\text{-}2,6\text{-}tBu_2\text{-}C_6H_3]$ is disordered and was refined in two positions. The crystal data and all of the bond lengths and angles for the independent molecules are available in the SI, and selected bond distances and angles for the independent molecules are listed in Table 2.

The geometries of $Lu[CH(SiMe_3)_2]_2[O\text{-}2,6\text{-}tBu_2\text{-}C_6H_3]$ and $Lu[CH(SiMe_3)_2][O\text{-}2,6\text{-}tBu_2\text{-}C_6H_3]_2$ are similar as the lutetium atoms lie in the plane defined by the carbon and oxygen atoms, which is in contrast to that in $Lu[CH(SiMe_3)_2]_3$ and $Lu[O\text{-}2,6\text{-}tBu_2\text{-}C_6H_3]_3$.[77] As the number of $[O\text{-}2,6\text{-}tBu\text{-}C_6H_3]$ groups in $Lu[CH(SiMe_3)_2]_{3-x}[O\text{-}2,6\text{-}tBu_2\text{-}C_6H_3]_x$ increases from one, to two, to three, the Lu−O distance slightly decreases from 2.032 ± 0.006 Å to 2.014 ± 0.004 Å to 2.013 ± 0.002 Å, respectively. The Lu−Cα distance does not change as the number of $[CH(SiMe_3)_2]$ ligands decreases from three to two to one; the values are 2.319(3), 2.32 ± 0.02, and 2.324 ± 0.007 Å, respectively. However, the Lu···Cγ distances shorten in the order of 2.937(3) Å to 2.69 ± 0.02 Å to 2.598 ± 0.008 Å as do the Lu···Siβ distances, 3.242(1) to 3.10 ± 0.01 Å to 3.048 ± 0.002 Å, respectively. These changes presumably reflect the

DOI: 10.1021/jacs.6b00071
J. Am. Chem. Soc. 2016, 138, 3831−3843

Table 2. Selected of Bond Lengths (Å) and Angles (°) for $Lu[CH(SiMe_3)_2]_3$, $Lu[CH(SiMe_3)_2]_2[O\text{-}2,6\text{-}tBu_2\text{-}C_6H_3]$, and $Lu[CH(SiMe_3)_2][O\text{-}2,6\text{-}tBu_2\text{-}C_6H_3]_2$

	M−Cα	M···Cγ	M···Siβ[a]	Siβ−Cγ	M−Cα−Siβ	Cα−Siβ−Cγ
$Lu[CH(SiMe_3)_2]_3$	2.319(3)	2.937(3)	3.242(1)	1.908(2)[b]	101.9(1)	106.7(1)
				1.871 ± 0.004[c]	125.7(4)	
$Lu[CH(SiMe_3)_2]_2[O\text{-}2,6\text{-}tBu_2\text{-}C_6H_3]$						
molecule 1	2.29(6)	2.67(1)	3.095(4)	1.89(1)[b]	96.8(7)	106.9(5)
					139.3(8)	
	2.32(1)	2.74(1)	3.111(4)	1.88(2)[c]	96.3(5)	106.0(6)
				1.87 ± 0.04[c]	133.0(6)	
molecule 2[d]	2.31(2)	2.71(4)	3.13(3)	2.01(3)[b]	99(1)	98(1)
					124(1)	
	2.33(2)	2.64(5)	3.07(1)	1.87(2)[b]	89(1)	103(1)
					138(1)	
	2.35(1)	2.69(1)	3.107(4)	1.93(1)[b]	94.6(6)	107.4(6)
				1.86 ± 0.03[c]	135.4(7)	
$Lu[CH(SiMe_3)_2][O\text{-}2,6\text{-}tBu_2\text{-}C_6H_3]_2$						
molecule 1	2.317(7)	2.595(7)	3.042(7)	1.917(7)[b]	93.0(3)	107.8(3)
				1.860 ± 0.008[c]	123.1(3)	
molecule 2	2.331(7)	2.601(8)	3.054(2)	1.917(7)[b]	93.3(9)	106.9(3)
				1.867 ± 0.007[c]	123.5(3)	

[a]Distance from Lu to the proximal Siβ. [b]Siβ−Cγ proximal to the lanthanide atom. [c]Average of all non-interacting Siβ−CγCγ. [d]One $-CH(SiMe_3)_2$ group refined in two positions.

electronegativity increase of oxygen relative to carbon, a conjecture that is corroborated by the NBO charges that are presented in the Computational Studies section.

Solution NMR Properties of $Lu[CH(SiMe_3)_2]_{3-x}[O\text{-}2,6\text{-}tBu_2\text{-}C_6H_3]_x$ (x = 0−2). The presence of short Lu···Cγ distances in $Lu[CH(SiMe_3)_2]_3$ implies that the chemically inequivalent $-SiMe_3$ groups should appear in a 3:3:3:9 ratio in the ^{1}H NMR spectrum.[78] The ^{1}H NMR spectrum of $Lu[CH(SiMe_3)_2]_3$ at 20 °C in methylcyclohexane-d_{14} contains a single sharp resonance for the $-SiMe_3$ groups at 0.36 ppm as does the ^{29}Si NMR spectrum at −8.6 ppm. The ^{13}C NMR spectrum at 20 °C contains two resonances at 59.8 ppm ($^1J_{CH}$ = 91 Hz) and at 5.6 ppm ($^1J_{CH}$ = 118 Hz) for the Lu-*C*α and the $-Si\mathit{Me}_3$ groups, respectively. These observations indicate that the $-SiMe_3$ groups are undergoing fast site exchange at this temperature. Cooling the sample in methylcyclohexane-d_{14} results in minimal line broadening until −100 °C. At −120 °C the resonance broadens but does not decoalesce, and the slow exchange limit is not reached in this solvent. However, further cooling a solution of $Lu[CH(SiMe_3)_2]_3$ in 2-methylbutane-d_{12} results in decoalesence at ca. −125 °C as two equal area resonances emerge, $\Delta G^{\ddagger}_{(T_c\,=\,148\ K)}$ = 7.1 kcal mol^{-1} (Figure S7a). At −140 °C the downfield resonance is broader than that of the upfield resonance indicating that rotation about the Cα−Siβ bonds is still rapid on the ^{1}H NMR time scale, but the rates are not equal. This result suggests that the downfield resonance is involved in the Lu···Cγ−Siβ interaction observed in the crystal structure. The variable-temperature ^{13}C{^{1}H} NMR spectra are qualitatively similar to the ^{1}H NMR spectra since the single $-SiMe_3$ resonance broadens by −125 °C and two distinct resonances emerge by −140 °C, the upfield resonance being broader than the downfield one, Figure S7b. The $^1J_{CH}$ coupling constants are 117 ± 1 Hz for both resonances in the chemically inequivalent $-SiMe_3$ groups at −140 °C.

In C_6D_6 solution, the ^{1}H NMR spectrum of $Lu[CH(SiMe_3)_2]_2[O\text{-}2,6\text{-}tBu_2\text{-}C_6H_3]$ contains a sharp signal at 0.33 ppm for the Lu−$CH(Si\mathit{Me}_3)_2$ groups, and the ^{13}C NMR spectrum has a resonance at 5.6 ppm due to these carbons. The $^1J_{CH}$ of the Lu−$CH(Si\mathit{Me}_3)_2$ group is 118 Hz, as in $Lu[CH(SiMe_3)_2]_3$. The lower solubility of $Lu[CH(SiMe_3)_2]_2[O\text{-}2,6\text{-}tBu_2\text{-}C_6H_3]$ in 2-methylbutane-d_{12} prohibits a quantitative study at very low temperatures, but qualitatively, $Lu[CH(SiMe_3)_2]_2[O\text{-}2,6\text{-}tBu_2\text{-}C_6H_3]$ has a similar profile as $Lu[CH(SiMe_3)_2]_3$. At −130 °C, the $-SiMe_3$ groups appear as three broad signals at 0.38, 0.28, and 0.041 ppm. These resonances coalesce at −120 °C indicating a low barrier for rotation of the Lu−Cα bond. Cooling the sample to −137 °C results in further line broadening, but the slow exchange limit is not reached (Figures S8 and S9). The combination of reduced solubility in 2-methylbutane-d_{12} and the intermediate exchange rates encountered in the variable-temperature ^{1}H NMR study inhibits a quantitative analysis of the ^{13}C NMR spectra at low temperatures.

The NMR spectra of $Lu[CH(SiMe_3)_2][O\text{-}2,6\text{-}tBu_2\text{-}C_6H_3]_2$ are similar to those of $Lu[CH(SiMe_3)_2]_2[O\text{-}2,6\text{-}tBu_2\text{-}C_6H_3]$ and $Lu[CH(SiMe_3)_3]_3$. The ^{1}H NMR spectrum of $Lu[CH(SiMe_3)_2][O\text{-}2,6\text{-}tBu_2\text{-}C_6H_3]_2$ in C_6D_6 at 20 °C contains sharp signals at 0.33 ppm for Lu−$C\mathit{H}(SiMe_3)_2$ and 0.050 ppm for Lu−$CH(Si\mathit{Me}_3)_2$, respectively, indicating fast site exchange between the two $-SiMe_3$ groups. The ^{13}C NMR spectrum contains a sharp signal for the methyl group at 4.8 ppm with $^1J_{CH}$ of 117 Hz. The monoalkyl is insoluble in 2-methylbutane-d_{12}, but the ^{1}H NMR spectrum in toluene-d_8 at −90 °C contains broad signals for the $-SiMe_3$ and $-t$Bu groups, indicating that the slow exchange limit is not reached by this temperature (Figure S10).

Solid-State NMR of $Lu[CH(SiMe_3)_2]_{3-x}[O\text{-}2,6\text{-}tBu_2\text{-}C_6H_3]_x$ (x = 0−2). Although the site exchange between the two $SiMe_3$ groups is slow below −125 °C in the solution ^{1}H spectrum of $Lu[CH(SiMe_3)_2]_3$, rotation about the Siβ−Cγ bond is still rapid at −140 °C. Although the solid-state crystal structure shows one short Lu···Cγ contact distance, this stereochemical feature is not resolved at −140 °C, and the nature of this interaction is not defined in solution. Solid-state NMR spectroscopy provides a definitive answer. The ^{29}Si

DOI: 10.1021/jacs.6b00071
J. Am. Chem. Soc. 2016, 138, 3831−3843

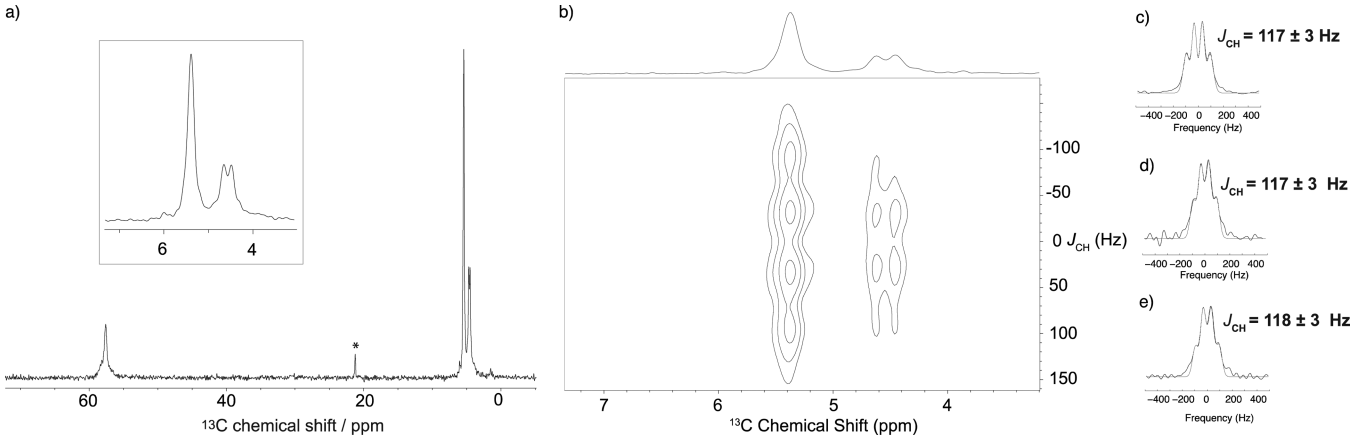

Figure 5. Solid-state NMR spectra of Lu[CH(SiMe$_3$)$_2$]$_3$. (a) ^{13}C CPMAS spectrum recorded at 12.5 kHz spinning frequency, the inset shows an expansion of the spectrum from 3−7 ppm, * = toluene. (b) 2D *J*-resolved spectrum of Lu[CH(SiMe$_3$)$_2$]$_3$ recorded at 12.5 kHz spinning frequency shown from 3−7 ppm. (c−e) 1D traces extracted from the 2D spectrum; the corresponding values of the J_{CH} coupling are given in the right-hand side. The black spectra are raw data, and the green spectra are best fits. The trace in (c) is from the signal at 5.4 ppm, the trace in (d) is from the signal at 4.7 ppm, and the trace in (e) is from the signal at 4.5 ppm. The experiments were carried out on a 700 MHz spectrometer. The recycle delay was 2 s, and a total of 42 t_1 increments of 1024 μs with 512 scans each were collected.

CPMAS spectrum of Lu[CH(SiMe$_3$)$_2$]$_3$ obtained at 5 kHz spinning speed contains two sharp signals at −5.3 and −11.7 ppm, indicating that the silicon atoms are inequivalent and that the rate of site exchange is slow in the solid state. The ^{13}C CPMAS spectrum of Lu[CH(SiMe$_3$)$_2$]$_3$ at 12.5 kHz, shown in Figure 5a, contains signals from Lu−*C*H(SiMe$_3$)$_2$ at 57.7 ppm and the Lu−CH(Si*Me*$_3$)$_2$ groups at 4.5, 4.7, and 5.4 ppm in a 1:1:4 area ratio at 20 °C. Assuming that the chemical shift of one SiMe is degenerate with that of the three equivalent SiMe$_3$ groups, the 1:1:4 pattern may be rationalize from the crystal structure, since the proximal −SiMe$_3$ group has C_1 local symmetry. The measurement of the ^{13}C refocused coherence lifetimes (using a CPMAS experiment followed by a spin echo period of variable delays) shows that the signals at 4.5 and 4.7 ppm have shorter T_2' values (32 and 31 ms, respectively) than the signal at 5.4 ppm (T_2' = 85 ms), indicating a more rigid environment or that conformational exchange is experienced by the signal at higher frequency (in line with the observation that the corresponding *J*-splitting are also slightly less resolved for these two peaks).

The solid-state *J*-resolved spectrum of Lu[CH(SiMe$_3$)$_2$]$_3$, shown in Figure 5b, gives nearly identical $^1J_{CH}$ values for each of the inequivalent −SiMe$_3$ group resonances, as shown in Figure 5c−e that are 1D traces extracted from the 2D spectrum, corroborating the solution data presented above. Similar results were obtained from the solid-state *J*-resolved spectra of Lu[CH(SiMe$_3$)$_2$]$_2$[O-2,6-*t*Bu$_2$-C$_6$H$_3$] and Lu[CH(SiMe$_3$)$_2$]-[O-2,6-*t*Bu$_2$-C$_6$H$_3$]$_2$ (Figures S14 and S17). These results indicate that agostic M···H−Cγ interactions are not present in solution nor in the solid state.

The chemical shift anisotropy (CSA) parameters associated with the chemically inequivalent −SiMe$_3$ groups contain information about the orientational dependence of the chemical shift tensor in an external magnetic field that relates to the anisotropic distribution of electron density at the specific nucleus in question. The CSA is characterized by the three principal components of a second rank tensor (δ_{11}, δ_{22}, δ_{33}). The isotropic chemical shift δ_{iso} is the average of the three components, $\delta_{iso} = 1/3(\delta_{11} + \delta_{22} + \delta_{33})$. As a result of rapid molecular tumbling, δ_{iso} is the only observable quantity in solution. The CSA is not averaged in solids and is directional, which results in a powder pattern from which the principal chemical shift components are obtained if sample spinning is slower than the magnitude of the CSA. The Herzfeld−Berger convention describes the span of the powder pattern Ω (Ω = $\delta_{11} - \delta_{33}$) and the skew κ ($\kappa = (\delta_{22} - \delta_{iso})/\Omega$).[79]

The ^{13}C CPMAS spectrum of Lu[CH(SiMe$_3$)$_2$]$_3$ at slow spinning speeds (1.5 kHz) shows that all of the −SiMe$_3$ resonances have very small values of the CSA that cannot be measured. However, the ^{29}Si CPMAS of Lu[CH(SiMe$_3$)$_2$]$_3$ obtained at 1.5 kHz spinning speed results in a manifold of spinning side bands, shown in Figure 6, from which extraction of the CSA parameters for each ^{29}Si NMR signal is possible. These values are given in Table 3. The signal at −5.3 ppm has principle components (δ_{11}, δ_{22}, δ_{33}) = (5.2, 4.1, −25.0) corresponding to a span Ω = 30.2, and the signal at −11.7 has principle components (δ_{11}, δ_{22}, δ_{33}) = (19.4, −27.1, −27.4) corresponding to a span Ω = 46.8. Both signals have similar skew (κ) values, though they differ in sign. The ^{29}Si CPMAS NMR spectrum of Lu[CH(SiMe$_3$)$_2$]$_2$[O-2,6-*t*Bu$_2$-C$_6$H$_3$] at 5 kHz spinning speed contains four signals at −3.1, −4.2, −11.8, and −12.7 ppm (Figure S18). The unit cell of Lu[CH-(SiMe$_3$)$_2$]$_2$[O-2,6-*t*Bu$_2$-C$_6$H$_3$] contains two independent molecules, which account for the presence of four signals in the ^{29}Si CPMAS NMR spectrum. The signals at −3.1 and −4.2 ppm are approximately in a 1:1 ratio as are the resonances at −11.8 and −12.7 ppm. Extracted CSA parameters at a slower spinning rate of 1.5 kHz are given in Table 3. The signals at −3.1 and −4.2 have principle components (δ_{11}, δ_{22}, δ_{33}) = (9.8, −0.8, −21.4) and (δ_{11}, δ_{22}, δ_{33}) = (9.0, 4.4, −22.9), respectively. These values correspond to a span Ω = 31.2 and 31.9 ppm, respectively. The signals at −11.8 and −12.7 have larger Ω values of 62.5 and 55.8 ppm, respectively.

The ^{29}Si CPMAS NMR spectrum of Lu[CH(SiMe$_3$)$_2$][O-2,6-*t*Bu$_2$-C$_6$H$_3$]$_2$, which also has two independent molecules in the unit cell, contains two sets of broad signals at −4.2 and −5.2 ppm as well as −12.8 and −13.6 ppm at 5 kHz spinning rate (Figure S20). The CSA parameters obtained from the ^{29}Si CPMAS NMR spectrum at 1.5 kHz sample spinning are summarized in Table 3. The resonances at −4.6 and −5.2 ppm have similar Ω of 30.3 and 28.3 ppm, while the signals at −12.8 and −13.6 have a Ω of 62.2 and 57.4 ppm, respectively.

DOI: 10.1021/jacs.6b00071
J. Am. Chem. Soc. 2016, 138, 3831−3843

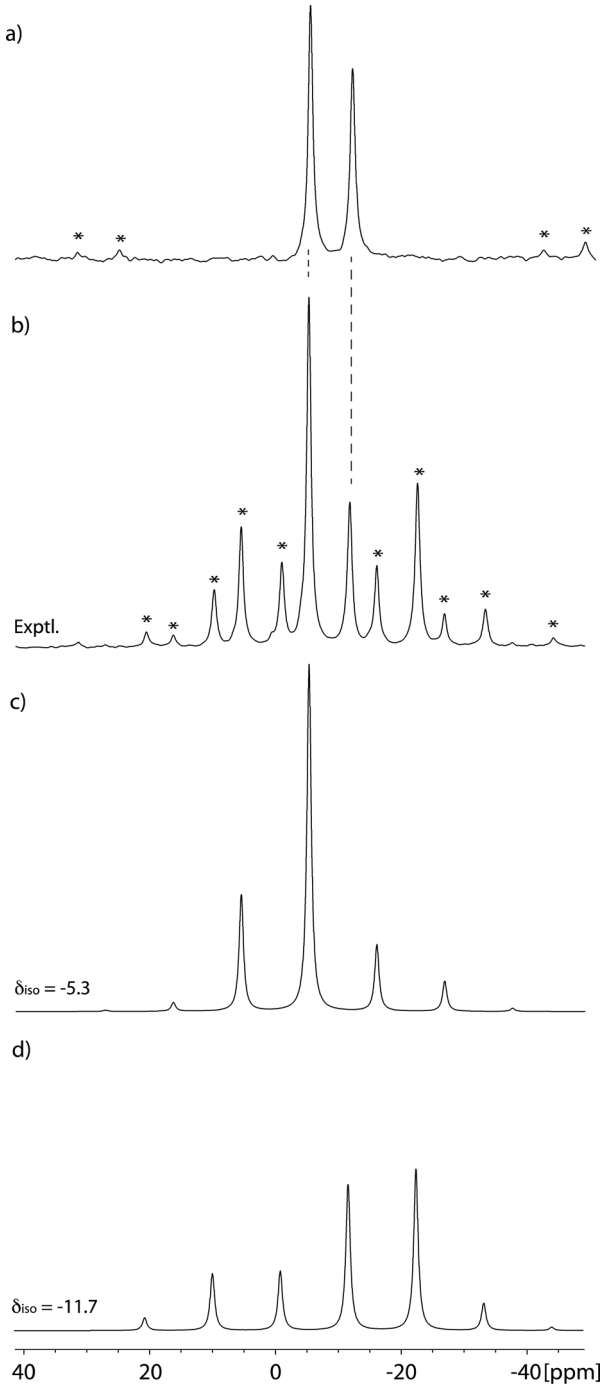

Figure 6. ^{29}Si CPMAS NMR spectrum of Lu[CH(SiMe$_3$)$_2$]$_3$: (a) 5 kHz and (b) 1.5 kHz spinning rates, both spectra were recorded with a 2 ms contact time; CSA fits for (c) the signal at −5.3 ppm and (d) the resonance at −11.7 ppm. The asterisks denote spinning side-bands.

The ^{29}Si NMR parameters of Lu[CH(SiMe$_3$)$_2$]$_3$, Lu[CH(SiMe$_3$)$_2$]$_2$[O-2,6-*t*Bu-C$_6$H$_3$], and Lu[CH(SiMe$_3$)$_2$][O-2,6-*t*Bu-C$_6$H$_3$]$_2$ follow the same pattern in which one silicon atom has a large span, while the other has a comparatively smaller span.

Computational Studies. The geometry of Lu[CH(SiMe$_3$)$_2$]$_3$, Lu[CH(SiMe$_3$)$_2$]$_2$[O-2,6-*t*Bu-C$_6$H$_3$], Lu[CH(SiMe$_3$)$_2$][O-2,6-*t*Bu-C$_6$H$_3$]$_2$, and Lu[O-2,6-*t*Bu-C$_6$H$_3$]$_3$ are optimized using DFT calculations. The computed geometries of the Lu-complexes are in good agreement with the solid-state structures independent of the functional used, though the Lu···Cγ distances are closest to the experimental values when small-core functionals that include dispersion are used (see the Supporting Information for details). The B3PW91-GD3BJ functional gives bond distances and angles closest to those found in their X-ray structures. Structures obtained using this functional are shown in Figure 7, and selected bond distances and angles are given in Table 4. The geometry of Lu[CH(SiMe$_3$)$_2$]$_2$[OSi(O*t*Bu)$_3$] is also calculated as a simple model for (≡SiO)Lu[CH(SiMe$_3$)$_2$]$_2$. Four geometries are located, one of which resembles the structure of Lu[CH(SiMe$_3$)$_2$]$_2$[O-2,6-*t*Bu-C$_6$H$_3$]. The others contain one short Lu···Cγ and one longer Lu···Cγ distance and/or the presence of Lu···O secondary interactions. The data for Lu[CH(SiMe$_3$)$_2$]$_2$[OSi(O*t*Bu)$_3$] are given in Figure S23 and Table S5.

The experimental ^{29}Si NMR parameters of Lu[CH(SiMe$_3$)$_2$]$_3$ contain one silicon with a large Ω span and one with a smaller span. The calculated ^{29}Si NMR CSA parameter for the distal Siβ in Lu[CH(SiMe$_3$)$_2$]$_3$ has δ_{iso} = −5.2 ppm with Ω = 29.7 and κ = 0.60, while the proximal Siβ has δ_{iso} = −13.5 with Ω = 51.6 and κ = −0.48. The values of δ_{iso} and Ω are close to those obtained experimentally, even though the calculated diagonal components of the second-rank tensors (δ_{11}, δ_{22}, δ_{33}) are not fully reproduced (see Table S4). In Lu[CH(SiMe$_3$)$_2$]$_2$[O-2,6-*t*Bu-C$_6$H$_3$] and Lu[CH(SiMe$_3$)$_2$][O-2,6-*t*Bu-C$_6$H$_3$]$_2$ a similar trend emerges. The Siβ proximal to Lu has a larger span value than the distal Siβ. These data are consistent with the postulate that the secondary Lu···CγSiβ interaction is associated with the larger anisotropy.

The natural charges on the atoms in the three calculated structures are shown in Table 5. The key message is that the Cγ carbon carries a partial negative charge, while the Hγ and Siβ's have partial positive charges, supporting the deduction that Lu···Cγ−Siβ is a 3c-2e interaction rather than a Lu···H−Cγ 3c-2e interaction. The trends in the NBO charges are remarkably constant for all atoms as C is replaced by −O-2,6-*t*Bu$_2$-C$_6$H$_3$, except for the positive charge on Lu, which increases slightly when the first C is replaced by −O-2,6-*t*Bu$_2$-C$_6$H$_3$, and somewhat more when the second C is replaced by −O-2,6-*t*Bu$_2$-C$_6$H$_3$. Replacing one C with −OSi(O^{t}Bu)$_3$ results in more positive charge on Lu (1.45−1.62 depending on the isomer) than replacing one C with −O-2,6-*t*Bu$_2$-C$_6$H$_3$ (see Table S6). This trend is coupled with a slight increase in negative charge on the proximal Cγ atoms as shown in Table 5. These data are consistent with an increase electrophilicity of the metal sites and illustrates how the ligands modulate the relative charges in a metal−ligand bond in accordance with the Pauling's electroneutrality principle.

DISCUSSION

The experimental and computational studies outlined above were motivated by the expectation that the electrophilicity of supported organometallic compounds on silica will increase relative to the molecular precursor.[35,80] The experimental studies begin with the characterization of [(≡SiO)Lu[CH(SiMe$_3$)$_2$]$_2$], which contains one short intramolecular Lu···Cγ contact distance of 2.80(2) Å. The Lu−Cγ distance is longer than the direct Lu−Cα distance of 2.32(1) Å and is classified as a secondary interaction.[1−3,81] In order to understand the nature of the secondary interactions in the supported compound, the structure of the surface species is compared with molecular compounds Lu[CH(SiMe$_3$)$_2$]$_3$, Lu[CH(SiMe$_3$)$_2$]$_2$[O-2,6-*t*Bu$_2$-C$_6$H$_3$], and Lu[CH(SiMe$_3$)$_2$][O-2,6-*t*Bu$_2$-C$_6$H$_3$]$_2$ that are

DOI: 10.1021/jacs.6b00071
J. Am. Chem. Soc. 2016, 138, 3831−3843

Table 3. CSA Parameters for the Signals in the ^{29}Si CPMAS NMR Spectrum of Lu[CH(SiMe$_3$)$_2$]$_3$, Lu[CH(SiMe$_3$)$_2$]$_2$[O-2,6-*t*Bu$_2$-C$_6$H$_3$], and Lu[CH(SiMe$_3$)$_2$][O-2,6-*t*Bu$_2$-C$_6$H$_3$]$_2$

	δ_{iso}	δ_{11}	δ_{22}	δ_{33}	Ω	κ
Lu[CH(SiMe$_3$)$_2$]$_3$	−5.3	5.21	4.11	−25.0	30.2	0.93
	−11.7	19.4	−27.1	−27.4	46.8	−0.98
Lu[CH(SiMe$_3$)$_2$]$_2$[O-2,6-*t*Bu-C$_6$H$_3$]	−3.1	9.8	−0.8	−21.4	31.2	0.32
	−4.2	9.0	4.4	−22.9	31.9	0.71
	−11.8	28.1	−29.1	−34.4	62.5	−0.83
	−12.7	22.3	−27.0	−33.5	55.8	−0.77
Lu[CH(SiMe$_3$)$_2$][O-2,6-*t*Bu-C$_6$H$_3$]$_2$	−4.3	15.6	−13.7	−14.8	30.3	−0.93
	−5.2	13.2	−13.6	−15.2	28.3	−0.80
	−12.8	24.4	−25.0	−37.8	62.2	−0.60
	−13.6	22.8	−28.9	−34.7	57.4	−0.80

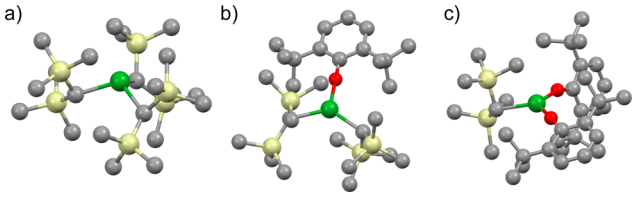

Figure 7. Calculated structures of Lu[CH(SiMe$_3$)$_2$]$_{3-x}$[O-2,6-*t*Bu-C$_6$H$_3$]$_x$ using B3PW91-GD3BJ: (a) Lu[CH(SiMe$_3$)$_2$]$_3$, (b) Lu[CH(SiMe$_3$)$_2$]$_2$[O-2,6-*t*Bu-C$_6$H$_3$], and (c) Lu[CH(SiMe$_3$)$_2$][O-2,6-*t*Bu-C$_6$H$_3$]$_2$.

studied by X-ray crystallography, NMR spectroscopy, and DFT calculations.

The M−C*α* and M−C*γ* distances in Ln[CH(SiMe$_3$)$_2$]$_3$ follow the general trend in metal radii, La[24] > Ce[23,82,83] > Sm[24] > Lu (this work) (Table 6). One exception is the Sm−C*γ* distance, but this distance has a large associated esd (Table 6). Contraction of the metal radius from La to Lu results in a La−C*α* distance that is 0.20 Å longer than that found for Lu, and the La···C*γ* distance is 0.19 Å longer than the equivalent distance in Lu. The difference between the Ln−C*α*−Si*β* angle in the proximal and distal −SiMe$_3$ groups of about 20° is essentially constant in the compounds listed in Table 6, as is the difference in the C*α*-Si*β*−C*γ* angles. The bond length and angle patterns are clear; short M···C*γ*−Si*β* distances are associated with more acute C*α*−Si*β*−C*γ* angles, and this distortion results in lengthening of one of the C*γ*−Si*β* bond distances; a similar pattern of distortions of the La−CH(SiMe$_3$)$_2$ group in Cp*La[CH(SiMe$_3$)$_2$]$_2$ are found by neutron diffraction.[76]

The solid-state crystal structure of Lu[CH(SiMe$_3$)$_2$]$_3$ shows that Lu lies out of the plane defined by the three carbon atoms by 0.81 Å. This distortion results in three methyl groups with short Lu···C*γ* contact distances, referred to as proximal methyl groups, while the other 15 methyl groups are distal. The Lu···C*γ* distances are approximately 0.38 Å longer than the Lu−C*α* distances, and the former are referred to as secondary bond distances.

This pattern in the geometry and the resulting classification of the Lu−C*α* and M···C*γ* distances is a general feature of the trialkyls listed in Table 6. X-ray determined H−C bond distances and torsional angles are helpful for making the distinction between 3c-2e M···H*γ*C*γ* or 3c-2e M···C*γ*Si*β* interaction when the hydrogen atoms are located and refined isotropically, but useless when the hydrogen atoms are placed in calculated positions and not refined. The C*γ*−Si*β* distances are in principle useful, but these distances are often statistically equal at the 3−5 *σ* confidence level. An experimental measurement that is capable of distinguishing between these two agostic models is the value of the $^1J_{CH}$ coupling constants

Table 5. Trends in NBO Charges

	Lu[CH(SiMe$_3$)$_2$]$_3$	Lu[CH(SiMe$_3$)$_2$]$_2$[O-2,6-*t*Bu-C$_6$H$_3$]	Lu[CH(SiMe$_3$)$_2$][O-2,6-*t*Bu-C$_6$H$_3$]$_2$
Lu	1.32	1.37	1.50
C*α*	−1.81	−1.80	−1.80
O	–	−0.86	−0.87
C*γ*[a]	−1.11	−1.14	−1.15
C*γ*′[b]	−1.12	−1.12	−1.12
Si*β*[a]	1.81	1.80	1.79
Si*β*′[b]	1.80	1.80	1.79
H*γ*[c]	0.25	0.27	0.26

[a]Proximal to Lu. [b]Average of all other values. [c]Hydrogens located on the proximal C*γ*.

Table 4. Selected Bond Lengths (Å) and Angles (°) of Lu[CH(SiMe$_3$)$_2$]$_x$[O-2,6-*t*Bu-C$_6$H$_3$]$_{3-x}$ (x = 1−3) and Using B3PW91-GD3BJ

	M−C*α*	M···C*γ*	M···Si*β*[a]	Si*β*−C*γ*	M−C*α*−Si*β*	C*α*−Si*β*−C*γ*
Lu[CH(SiMe$_3$)$_2$]$_3$	2.289	2.942[b]	3.220[b]	1.916[c]	101.7	106.5
				1.885[d]	124.7	
Lu[CH(SiMe$_3$)$_2$]$_2$[O-2,6-*t*Bu$_2$-C$_6$H$_3$]	2.311	2.640	3.054	1.938[c]	93.8	107.4
				1.884[d]	131.9	
	2.314	2.636	3.061	1.937[c]	94.0	109.6
				1.884[d]	132.8	
Lu[CH(SiMe$_3$)$_2$][O-2,6-*t*Bu$_2$-C$_6$H$_3$]$_2$	2.319	2.579	3.009	1.955[c]	91.8	108.2
				1.884[d]	119.7	

[a]Distance from Lu to the proximal Si*β*. [b]Average of three distances; a full table of all distances and angles is provided in the Supporting Information. [c]Average Si*β*−C*γ* proximal to the lanthanide atom. [d]Average of all other Si*β*−C*γ*.

DOI: 10.1021/jacs.6b00071
J. Am. Chem. Soc. 2016, 138, 3831−3843

Table 6. Comparison of Bond Lengths (Å) and Angles (°) for $Ln[CH(SiMe_3)_2]_3$

Ln	M−Cα	M···Cγ	M···Siβ	Siβ−Cγ	M−Cα-Siβ	Cα-Siβ−Cγ	ref
Y	2.353(5)	2.963(6)	3.284(2)	1.925(5)[a]	102.1(2)	106.6(3)	23
				1.875 ± 0.001[b]	126.3(3)		
La	2.515(9)	3.121(9)	3.410(2)	1.923(1)[a]	102.0(4)	109.7(5)	22
				1.866 ± 0.001[b]	121.0(4)		
Ce	2.475(7)	3.068(7)	3.3884(3)	1.9251(1)[a]	102.8(3)	108.2(4)	23
				1.887 ± 0.001[b]	122.3(4)		
Sm	2.33(2)	2.85(3)	3.325(6)	1.946(1)[a]	107(1)	105(1)	22
				1.882 ± 0.001[b,c]	124(1)		
Lu	2.318(2)	2.936(2)	3.242(1)	1.908(2)[a]	101.9(1)	106.7(1)	this work
				1.871 ± 0.004[b]	125.8(1)		

[a]Siβ−Cγ proximal to the lanthanide atom. [b]Average of all Siβ−Cγ. [c]One unusually long distal Si−Me (1.950 Å) is not included in this average distance.

when the fluxionality between proximal and distal Me_3Si groups is slow. In this case $^1J_{CH}$ provides unequivocal experimental evidence about the nature of the C−H bonds. In solution $Lu[CH(SiMe_3)_2]_3$ is fluxional in the ^{1}H NMR spectrum down to −100 °C, but the $-SiMe_3$ groups decoalesce by −125 °C into two chemically inequivalent, equal area resonances by −140 °C. The chemical inequivalence of the $-SiMe_3$ groups is consistent with the solid-state X-ray crystal structure, but does not provide information on the nature of the interaction. The $^{13}C\{^1H\}$ chemical shifts follow a similar pattern as the ^{1}H chemical shifts as a function of temperature. The proton coupled ^{13}C NMR spectrum provides the important detail that the $^1J_{CH}$ coupling constants do not change significantly from 20 to −140 °C; at 20 °C, $^1J_{CH}$ is 118 Hz, and at −140 °C, $^1J_{CH}$ is 117 and 116 Hz in the chemically inequivalent $-SiMe_3$ groups. These results are consistent with sp^3-hybridized carbons on the proximal and distal $-SiMe_3$ groups. At −140 °C, the slow exchange limit, which would result in four ^{13}C resonances in a 1:1:1:3 ratio, is not reached indicating that rotation around the Siβ−Cγ bond is still rapid at this temperature. Similar trends are found for $Lu[CH(SiMe_3)_2]_2[O\text{-}2,6\text{-}t\text{Bu-}C_3H_6]$ and $Lu[CH(SiMe_3)_2][O\text{-}2,6\text{-}t\text{Bu-}C_3H_6]_2$.

The value of $^1J_{CH}$ for Cα in $Lu[CH(SiMe_3)_2]_3$, $Lu[CH(SiMe_3)_2]_2[O\text{-}2,6\text{-}t\text{Bu-}C_3H_6]$, and $Lu[CH(SiMe_3)_2][O\text{-}2,6\text{-}t\text{Bu-}C_3H_6]_2$ ranges from 91 to 96 Hz, substantially reduced relative to the $^1J_{CH}$ for the $-SiMe_3$ groups (118 Hz). At first glance this might imply an agostic Lu···HαCα interaction. However, since lutetium is an electropositive metal atom, the s-electron density at Cα is polarized toward Lu, and accordingly more p-character is present in the C−H bond, lowering $^1J_{CH}$. This application of Bent's rule is an alternative explanation for the general observation of low values of $^1J_{CH}$ in electropositive main group elements.[84]

The solid-state ^{13}C CPMAS NMR spectrum of $Lu[CH(SiMe_3)_2]_3$ at 20 °C provides definitive evidence about the nature of the Lu···Cγ interaction. The spectrum shows that the methyl resonances are resolved into three distinct resonances in the area ratio of 4:1:1 (12:3:3) (Figure 5a). This pattern indicates that one Me_3Si group contains three chemically equivalent methyl groups, while the other contains three chemically inequivalent methyl groups, assuming that one resonance in the latter grouping is hidden under the former resonance. A physical process that accounts for this behavior is that rotation about one Siβ−Cα bond is free, while the other is restricted. We also observed that the two inequivalent $-SiMe_3$ sites have significantly shorter ^{13}C transverse coherence lifetimes (T_2' of 32 and 31 ms, respectively) compared to the equivalent $-SiMe_3$ sites (T_2' = 85 ms), which is consistent with a more rigid structure of the inequivalent $-SiMe_3$ group, due to their interaction with Lu or to a homogeneous broadening due to conformational exchange. Further, the solid-state *J*-resolved spectrum gives equal $^1J_{CH}$ values for the three resonances, indicating a lack of asymmetry in the C−H bonds, which in turn requires that the carbon in each Si−Me group is sp^3 hybridized.

Although we were unable to measure the CSA in the ^{13}C CPMAS spectrum, which may be due to the largely unperturbed sp^3 hybridized γ-carbon, the solid-state ^{29}Si NMR spectra of $Lu[CH(SiMe_3)_2]_3$, $Lu[CH(SiMe_3)_2]_2[O\text{-}2,6\text{-}t\text{Bu-}C_3H_6]$, and $Lu[CH(SiMe_3)_2][O\text{-}2,6\text{-}t\text{Bu-}C_3H_6]_2$ contain two silicon environments in a 1:1 area ratio. In this case the CSA of both silicon atoms can be measured: one ^{29}Si NMR resonance has a narrow span (the value of Ω) indicating a more or less symmetrical silicon environment, while the other has a significantly larger Ω value indicating a more asymmetric silicon environment, which is most reasonably ascribed to the presence of the Lu···Cγ−Siβ interaction. A Newman projection, Scheme 3, viewed down the Siβ−Cα bond is a pictorial representation of these solid-state NMR results.

Scheme 3. Newman Projection Viewed Down the Siβ−Cα Bond Showing the Lu···Cγ−Siβ Agostic Interaction

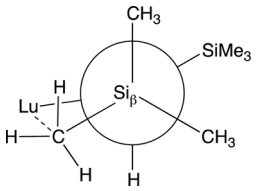

The NBO charges provide the final, and perhaps the most convincing, evidence that distinguishes between 3c-2e M···Cγ−Siβ or M···Hγ−Cγ interactions. The NBO charges on silicon in the $-SiMe_3$ groups are large and positive, and those on the hydrogen atoms are much smaller but still positive. The charge on the Cγ atoms is negative as is the charge on Cα, which is directly bonded to the positively charged Lu. Although the C atoms carry negative charges, the value on Cγ is about 40% less than that on Cα, consistent with classification of the former as a secondary bonding interaction and the latter as a primary one. The relative signs of the NBO charges clearly indicate that the Lu−Cα and Lu···Cγ are attractive interactions, while the Lu···Siβ and Lu···Hγ are repulsive.

DOI: 10.1021/jacs.6b00071
J. Am. Chem. Soc. 2016, 138, 3831−3843

The motivation for the studies outlined in this article is to develop and use the physical properties of molecular compounds as structural models for how a solid silica support influences the physical properties of the Lu−CH(SiMe$_3$)$_2$ fragment in (≡SiO)Lu[CH(SiMe$_3$)$_2$]$_2$. When comparing molecular and surface species, one can see that in (≡SiO)Lu[CH(SiMe$_3$)$_2$]$_2$ the distance for the Lu···Cγ interaction lies in between those of Lu[CH(SiMe$_3$)$_2$]$_3$ and Lu[CH(SiMe$_3$)$_2$]$_2$[O-2,6-tBu$_2$-C$_3$H$_6$], which is consistent with the similar calculated proton affinity between the two hydroxyls: 339.5 kcal mol^{-1} for [HO-2,6-tBu$_2$-C$_3$H$_6$] and 349.5 kcal mol^{-1} for HOSi(OR)$_3$. However, in contrast to the molecular species studied experimentally and computationally, (≡SiO)Lu[CH(SiMe$_3$)$_2$]$_2$ has an extra O-neighbor observed by EXAFS due to the presence of adjacent siloxane bridges. The presence of the Lu···Cγ interaction indicates that the electrophilicity of lutetium increases on grafting on silica, and the increase is presumably the reason for the short Lu···O interaction with a SiOSi group on the surface. In addition, the ^{29}Si NMR spectrum of (≡SiO)Lu[CH(SiMe$_3$)$_2$]$_2$ indicates that the Lu−CH(SiMe$_3$)$_2$ fragments are dynamic, which is commonly observed in monografted silica-supported organometallics.[85]

CONCLUSIONS

The results outline above lead to the inescapable conclusion that the nature of the short Lu···Cγ distance in Lu[CH(SiMe$_3$)$_2$]$_x$[O-2,6-tBu$_2$-C$_3$H$_6$]$_{3-x}$ is not due to a Lu···H−Cγ agostic interaction but to a Lu···Cγ−Siβ interaction in which the methyl group bridges the lutetium and silicon atoms.[74,75] The electron density in the CγSiβ σ-bond provides the electron density for the three-centered molecular orbital, as suggested by Morokuma.[73] A recent review by two of the original authors responsible for coining the adjective "agostic" states that the adjective agostic is inappropriate for such an interaction since agostic specifically refers to 3c-2e interactions involving M···H−C bonds and does not apply to all 3c-2e bonds.[3] The classification of M···C distances as 3c-2e M···H−C agostic, rather than as a 3c-2e bridging methyl interactions, brings to mind the argument about the bonding in Me$_4$Al$_2$(μ-Me$_2$)$_2$. The original formulation by Longuet-Higgins[86] was that the μ-Me is a 3c-2e bridge bond analogous to his model for the bridging hydrogens in B$_2$H$_6$. An alternative model formulated the bridging methyl as a 3c-2e Al···H−C bond on the basis of X-ray diffraction data in which the hydrogen atoms were neither located nor refined.[87] Cotton pointed out that the reformulation was "unjustified, incorrect, and misleading".[88] A low-temperature X-ray data set was obtained, in which the hydrogen atoms were located and refined,[89] is consistent with the Lougnet-Higgins model. An extension of the model by Morokuma,[73,90,91] which was used to explain the bonding between Ti and the γ-methyl group in Cp$_2$Ti−C(SiMe$_3$)=C(Me)(Ph)$^+$, is applied to the interaction between Lu and a γ-methyl group in Lu[CH(SiMe$_3$)$_2$]$_3$ and related compounds (Table 6). The Lu···Cγ distance in (≡SiO)Lu[CH(SiMe$_3$)$_2$]$_2$ lies in between that found in Lu[CH(SiMe$_3$)$_2$]$_3$ and in Lu[CH(SiMe$_3$)$_2$]$_2$[O-2,6-tBu-C$_6$H$_3$]. The Lu−Cγ distance gets shorter as the number of oxygen-containing ligands increase and is modulated by the siloxane bridge in the silica-supported compound. This interaction is associated with the increase of positive charge on Lu and therefore with the increase in electrophilicity at the metal sites. This interaction is particularly favorable in the compounds described in this article since Lu is three-coordinate and coordinatively unsaturated in absence of secondary interactions. The Lu−Cγ interaction also demonstrates the effect of introducing a surface siloxy ligand in the coordination sphere of a low coordinate metal site and shows how silica modulates the electrophilicity of surface sites by making them better Lewis acids. The use of solid-state NMR spectroscopy illustrates the power of this technique to provide details about structure and bonding in molecular and surface species.[85,92−97] Future studies will develop this theme.

ASSOCIATED CONTENT

Supporting Information

The Supporting Information is available free of charge on the ACS Publications website at DOI: 10.1021/jacs.6b00071.

Crystallographic data (CIF)
Crystallographic data (CIF)
Crystallographic data (CIF)
(PDB)
(PDB)
(PDB)
(PDB)
(PDB)
(PDB)
(PDB)
Solution NMR, additional solid-state NMR spectra, crystallographic tables, computational details (PDF)

AUTHOR INFORMATION

Corresponding Authors

*ccoperet@ethz.ch
*raandersen@lbl.gov

Notes

The authors declare no competing financial interest.

ACKNOWLEDGMENTS

C.C. thanks the Miller Institute for a Visiting Professor position at UC Berkeley, during which this manuscript was finalized. Portions of this work were performed at Lawrence Berkeley National Laboratory under contract no. DE-AC02-05CH11231 and at the Stanford Synchrotron Radiation Lightsource (SSRL). Use of the Stanford Synchrotron Radiation Lightsource, SLAC National Accelerator Laboratory, is supported by the U.S. Department of Energy, Office of Science, Office of Basic Energy Sciences under contract no. DE-AC02-76SF00515. Portions of this work were supported by the U.S. Department of Energy, Office of Science, Basic Energy Sciences, Chemical Sciences, Biosciences, and Geosciences Division (CSGB), Heavy Element Chemistry Program and were performed at Lawrence Berkeley National Laboratory under contract no. DE-AC02-05CH11231. We also thank the HPCs CALcul en Midi-Pyrennes (CALIMP-EOS, grant P0833) for the generous allocation of computer time. Financial support from the TGIR-RMN-THC Fr3050 CNRS for conducting the research is gratefully acknowledged.

REFERENCES

(1) Brookhart, M.; Green, M. L. H. *J. Organomet. Chem.* **1983**, *250*, 395.
(2) Brookhart, M.; Green, M. L. H.; Wong, L. L. *Prog. Inorg. Chem.* **1988**, *36*, 1.
(3) Brookhart, M.; Green, M. L. H.; Parkin, G. *Proc. Natl. Acad. Sci. U. S. A.* **2007**, *104*, 6908.
(4) Coates, G. W. *Chem. Rev.* **2000**, *100*, 1223.

DOI: 10.1021/jacs.6b00071
J. Am. Chem. Soc. 2016, 138, 3831−3843

(5) Grubbs, R. H.; Coates, G. W. *Acc. Chem. Res.* **1996**, *29*, 85.
(6) Brintzinger, H. H.; Fischer, D.; Mülhaupt, R.; Rieger, B.; Waymouth, R. M. *Angew. Chem., Int. Ed. Engl.* **1995**, *34*, 1143.
(7) Ittel, S. D.; Johnson, L. K.; Brookhart, M. *Chem. Rev.* **2000**, *100*, 1169.
(8) Oskam, J. H.; Schrock, R. R. *J. Am. Chem. Soc.* **1993**, *115*, 11831.
(9) Jeong, H.; John, J. M.; Schrock, R. R.; Hoveyda, A. H. *J. Am. Chem. Soc.* **2015**, *137*, 2239.
(10) Jeong, H.; John, J. M.; Schrock, R. R. *Organometallics* **2015**, *34*, 5136.
(11) Schrock, R. R.; Crowe, W. E.; Bazan, G. C.; DiMare, M.; O'Regan, M. B.; Schofield, M. H. *Organometallics* **1991**, *10*, 1832.
(12) Schrock, R. R. *Chem. Rev.* **2009**, *109*, 3211.
(13) Oskam, J. H.; Schrock, R. R. *J. Am. Chem. Soc.* **1992**, *114*, 7588.
(14) Flook, M. M.; Borner, J.; Kilyanek, S. M.; Gerber, L. C. H.; Schrock, R. R. *Organometallics* **2012**, *31*, 6231.
(15) Hartwig, J. F. *Organotransition Metal Chemistry: From Bonding to Catalysis*; University Science Books: South Orange, New Jersey, 2010.
(16) Perutz, R. N.; Sabo-Etienne, S. *Angew. Chem., Int. Ed.* **2007**, *46*, 2578.
(17) Dawoodi, Z.; Green, M. L. H.; Mtetwa, V. S. B.; Prout, K.; Schultz, A. J.; Williams, J. M.; Koetzle, T. F. *J. Chem. Soc., Dalton Trans.* **1986**, 1629.
(18) Dawoodi, Z.; Green, M. L. H.; Mtetwa, V. S. B.; Prout, K. *J. Chem. Soc., Chem. Commun.* **1982**, 802.
(19) Solans-Monfort, X.; Clot, E.; Copéret, C.; Eisenstein, O. *Organometallics* **2005**, *24*, 1586.
(20) Poater, A.; Solans-Monfort, X.; Clot, E.; Copéret, C.; Eisenstein, O. *Dalton Trans.* **2006**, 3077.
(21) Brookhart, M.; Green, M. L. H.; Pardy, R. B. A. *J. Chem. Soc., Chem. Commun.* **1983**, 691.
(22) For a review on related C−C secondary interactions, see: Etienne, M.; Weller, A. S. *Chem. Soc. Rev.* **2014**, *43*, 242.
(23) Avent, A. G.; Caro, C. F.; Hitchcock, P. B.; Lappert, M. F.; Li, Z.; Wei, X.-H. *Dalton Trans.* **2004**, 1567.
(24) Hitchcock, P. B.; Lappert, M. F.; Smith, R. G.; Bartlett, R. A.; Power, P. P. *J. Chem. Soc., Chem. Commun.* **1988**, 1007.
(25) Jeske, G.; Lauke, H.; Mauermann, H.; Swepston, P. N.; Schumann, H.; Marks, T. J. *J. Am. Chem. Soc.* **1985**, *107*, 8091.
(26) Stern, D.; Sabat, M.; Marks, T. J. *J. Am. Chem. Soc.* **1990**, *112*, 9558.
(27) Giardello, M. A.; Conticello, V. P.; Brard, L.; Sabat, M.; Rheingold, A. L.; Stern, C. L.; Marks, T. J. *J. Am. Chem. Soc.* **1994**, *116*, 10212.
(28) Schaverien, C. J.; Orpen, A. G. *Inorg. Chem.* **1991**, *30*, 4968.
(29) Cheng, J.; Takats, J.; Ferguson, M. J.; McDonald, R. *J. Am. Chem. Soc.* **2008**, *130*, 1544.
(30) Tian, S.; Arredondo, V. M.; Stern, C. L.; Marks, T. J. *Organometallics* **1999**, *18*, 2568.
(31) Heeres, H. J.; Renkema, J.; Booij, M.; Meetsma, A.; Teuben, J. H. *Organometallics* **1988**, *7*, 2495.
(32) Schumann, H.; Rosenthal, E. C. E.; Kociok-Kohn, G.; Molander, G. A.; Winterfeld, J. *J. Organomet. Chem.* **1995**, *496*, 233.
(33) Schaverien, C. J.; Nesbitt, G. J. *J. Chem. Soc., Dalton Trans.* **1992**, 157.
(34) Copéret, C.; Chabanas, M.; Petroff Saint-Arroman, R.; Basset, J.-M. *Angew. Chem., Int. Ed.* **2003**, *42*, 156.
(35) Rascon, F.; Wischert, R.; Copéret, C. *Chem. Sci.* **2011**, *2*, 1449.
(36) Gajan, D.; Copéret, C. *New J. Chem.* **2011**, *35*, 2403.
(37) Conley, M.; Copéret, C. *Top. Catal.* **2014**, *57*, 843.
(38) Copéret, C.; Comas-Vives, A.; Conley, M. P.; Estes, D. P.; Fedorov, A.; Mougel, V.; Nagae, H.; Nunez-Zarur, F.; Zhizhko, P. A. *Chem. Rev.* **2016**, *116*, 323.
(39) Bradley, D. C.; Ghotra, J. S.; Hart, F. A. *J. Chem. Soc., Dalton Trans.* **1973**, 1021.
(40) Lappert, M. F.; Singh, A.; Smith, R. G.; Stecher, H. A.; Sen, A. In *Inorganic Syntheses*; John Wiley & Sons, Inc.: Hoboken, NJ, 2007; p 164.
(41) Le Roux, E.; Chabanas, M.; Baudouin, A.; de Mallmann, A.; Copéret, C.; Quadrelli, E. A.; Thivolle-Cazat, J.; Basset, J.-M.; Lukens, W.; Lesage, A.; Emsley, L.; Sunley, G. J. *J. Am. Chem. Soc.* **2004**, *126*, 13391.
(42) Lesage, A.; Emsley, L.; Chabanas, M.; Copéret, C.; Basset, J.-M. *Angew. Chem., Int. Ed.* **2002**, *41*, 4535.
(43) Elena, B.; de Paepe, G.; Emsley, L. *Chem. Phys. Lett.* **2004**, *398*, 532.
(44) Fung, B. M.; Khitrin, A. K.; Ermolaev, K. *J. Magn. Reson.* **2000**, *142*, 97.
(45) Metz, G.; Wu, X. L.; Smith, S. O. *J. Magn. Reson., Ser. A* **1994**, *110*, 219.
(46) Ravel, B.; Newville, M. *Phys. Scr.* **2005**, *2005*, 1007.
(47) Newville, M. *J. Synchrotron Radiat.* **2001**, *8*, 322.
(48) Zabinsky, S. I.; Rehr, J. J.; Ankudinov, A.; Albers, R. C.; Eller, M. J. *Phys. Rev. B: Condens. Matter Mater. Phys.* **1995**, *52*, 2995.
(49) Frisch, M. J. Trucks, G. W.; Schlegel, H. B.; Scuseria, G. E.; Robb, M. A.; Cheeseman, J. R.; Scalmani, G.; Barone, V.; Mennucci, B.; Petersson, G. A.; Nakatsuji, H.; Caricato, M.; Li, X.; Hratchian, H. P.; Izmaylov, A. F.; Bloino, J.; Zheng, G.; Sonnenberg, J. L.; Hada, M.; Ehara, M.; Toyota, K.; Fukuda, R.; Hasegawa, J.; Ishida, M.; Nakajima, T.; Honda, Y.; Kitao, O.; Nakai, H.; Vreven, T.; Montgomery, J. A., Jr.; Peralta, J. E.; Ogliaro, F.; Bearpark, M.; Heyd, J. J.; Brothers, E.; Kudin, K. N.; Staroverov, V. N.; Kobayashi, R.; Normand, J.; Raghavachari, K.; Rendell, A.; Burant, J. C.; Iyengar, S. S.; Tomasi, J.; Cossi, M.; Rega, N.; Millam, J. M.; Klene, M.; Knox, J. E.; Cross, J. B.; Bakken, V.; Adamo, C.; Jaramillo, J.; Gomperts, R.; Stratmann, R. E.; Yazyev, O.; Austin, A. J.; Cammi, R.; Pomelli, C.; Ochterski, J. W.; Martin, R. L.; Morokuma, K.; Zakrzewski, V. G.; Voth, G. A.; Salvador, P.; Dannenberg, J. J.; Dapprich, S.; Daniels, A. D.; Farkas, Ö.; Foresman, J. B.; Ortiz, J. V.; Cioslowski, J.; Fox, D. J. *Gaussian 09*; Gaussian, Inc.: Wallingford, CT, 2009.
(50) Perdew, J. P.; Ziesche, P.; Eschrig, H. *Electronic structure of solids,'91*; Akademie Verlag, Berlin, 1991; Vol. *11*.
(51) Perdew, J. P.; Burke, K.; Wang, Y. *Phys. Rev. B: Condens. Matter Mater. Phys.* **1996**, *54*, 16533.
(52) Perdew, J. P.; Chevary, J. A.; Vosko, S. H.; Jackson, K. A.; Pederson, M. R.; Singh, D. J.; Fiolhais, C. *Phys. Rev. B: Condens. Matter Mater. Phys.* **1992**, *46*, 6671.
(53) Perdew, J. P.; Burke, K.; Wang, Y. *Phys. Rev. B: Condens. Matter Mater. Phys.* **1998**, *57*, 14999.
(54) Perdew, J. P.; Chevary, J. A.; Vosko, S. H.; Jackson, K. A.; Pederson, M. R.; Singh, D. J.; Fiolhais, C. *Phys. Rev. B: Condens. Matter Mater. Phys.* **1993**, *48*, 4978.
(55) Cao, X.; Dolg, M. *J. Mol. Struct.: THEOCHEM* **2002**, *581*, 139.
(56) Dolg, M.; Stoll, H.; Preuss, H. *J. Chem. Phys.* **1989**, *90*, 1730.
(57) Hariharan, P. C.; Pople, J. A. *Theor. Chim. Acta* **1973**, *28*, 213.
(58) Hehre, W. J.; Ditchfield, R.; Pople, J. A. *J. Chem. Phys.* **1972**, *56*, 2257.
(59) Dunning, T. H. *J. Chem. Phys.* **1989**, *90*, 1007.
(60) London, F. *J. Phys. Radium* **1937**, *8*, 397.
(61) McWeeny, R. *Phys. Rev.* **1962**, *126*, 1028.
(62) Ditchfield, R. *Mol. Phys.* **1974**, *27*, 789.
(63) Dodds, J. L.; McWeeny, R.; Sadlej, A. J. *Mol. Phys.* **1977**, *34*, 1779.
(64) Reed, A. E.; Weinhold, F. *J. Chem. Phys.* **1983**, *78*, 4066.
(65) Reed, A. E.; Curtiss, L. A.; Weinhold, F. *Chem. Rev.* **1988**, *88*, 899.
(66) Cowley, A. H.; Kemp, R. A. *Synth. React. Inorg. Met.-Org. Chem.* **1981**, *11*, 591.
(67) Davidson, P. J.; Harris, D. H.; Lappert, M. F. *J. Chem. Soc., Dalton Trans.* **1976**, 2268.
(68) Giesbrecht, G. R.; Gordon, J. C.; Clark, D. L.; Scott, B. L. *Inorg. Chem.* **2004**, *43*, 1065.
(69) Konkol, M.; Spaniol, T. P.; Kondracka, M.; Okuda, J. *Dalton Trans.* **2007**, 4095.
(70) Fischbach, A.; Herdtweek, E.; Anwander, R.; Eickerling, G.; Scherer, W. *Organometallics* **2003**, *22*, 499.

DOI: 10.1021/jacs.6b00071
J. Am. Chem. Soc. 2016, 138, 3831−3843

(71) The model with a single carbon neighbor at 2.80 Å fits the data better than the model with a single oxygen atom. However, a model with 0.8 oxygen atoms also provides a good fit. Using EXAFS it is not possible to distinguish a single carbon neighbor from 0.8 oxygen neighbors.
(72) Scherer, W.; McGrady, G. S. *Angew. Chem., Int. Ed.* **2004**, *43*, 1782.
(73) Koga, N.; Morokuma, K. *J. Am. Chem. Soc.* **1988**, *110*, 108.
(74) Tilley, T. D.; Andersen, R. A.; Zalkin, A. *J. Am. Chem. Soc.* **1982**, *104*, 3725.
(75) Rozenel, S. S.; Andersen, R. A. *Inorg. Chim. Acta* **2014**, *422*, 202.
(76) Klooster, W. T.; Brammer, L.; Schaverien, C. J.; Budzelaar, P. H. M. *J. Am. Chem. Soc.* **1999**, *121*, 1381.
(77) Steele, L. A. M.; Boyle, T. J.; Kemp, R. A.; Moore, C. *Polyhedron* **2012**, *42*, 258.
(78) Stoebenau, E. J., III; Jordan, R. F. *J. Organomet. Chem.* **2006**, *691*, 4956.
(79) Herzfeld, J.; Berger, A. E. *J. Chem. Phys.* **1980**, *73*, 6021.
(80) Ballard, D. G. H. In *Advances in Catalysis*; D.D. Eley, H. P., Paul, B. W., Eds.; Academic Press: Cambridge, MA, 1973; Vol. *23*, p 263.
(81) Clot, E.; Eisenstein, O. *Struct. Bonding* **2004**, *113*, 1.
(82) Heeres, H. J.; Teuben, J. H.; Rogers, R. D. *J. Organomet. Chem.* **1989**, *364*, 87.
(83) Booij, M.; Kiers, N. H.; Heeres, H. J.; Teuben, J. H. *J. Organomet. Chem.* **1989**, *364*, 79.
(84) Mann, B. E.; Taylor, B. F. *^{13}C NMR data for organometallic compounds*; Academic Press: Cambridge, MA, 1981.
(85) Blanc, F.; Basset, J.-M.; Copéret, C.; Sinha, A.; Tonzetich, Z. J.; Schrock, R. R.; Solans-Monfort, X.; Clot, E.; Eisenstein, O.; Lesage, A.; Emsley, L. *J. Am. Chem. Soc.* **2008**, *130*, 5886.
(86) Longuet-Higgins, H. C. *J. Chem. Soc.* **1946**, 139.
(87) Byram, S. K.; Fawcett, J. K.; Nyburg, S. C.; O'Brien, R. J. *J. Chem. Soc. D* **1970**, 16.
(88) Cotton, F. A. *Inorg. Chem.* **1970**, *9*, 2804.
(89) Huffman, J. C.; Streib, W. E. *J. Chem. Soc. D* **1971**, 911.
(90) Mitoraj, M. P.; Michalak, A.; Ziegler, T. *Organometallics* **2009**, *28*, 3727.
(91) Perrin, L.; Maron, L.; Eisenstein, O.; Lappert, M. F. *New J. Chem.* **2003**, *27*, 121.
(92) Blanc, F.; Copéret, C.; Lesage, A.; Emsley, L. *Chem. Soc. Rev.* **2008**, *37*, 518.
(93) Smart, K. A.; Grellier, M.; Coppel, Y.; Vendier, L.; Mason, S. A.; Capelli, S. C.; Albinati, A.; Montiel-Palma, V.; Munoz-Hernandez, M. A.; Sabo-Etienne, S. *Inorg. Chem.* **2014**, *53*, 1156.
(94) Pike, S. D.; Chadwick, F. M.; Rees, N. H.; Scott, M. P.; Weller, A. S.; Kramer, T.; Macgregor, S. A. *J. Am. Chem. Soc.* **2015**, *137*, 820.
(95) Lucier, B. E. G.; Johnston, K. E.; Xu, W.; Hanson, J. C.; Senanayake, S. D.; Yao, S.; Bourassa, M. W.; Srebro, M.; Autschbach, J.; Schurko, R. W. *J. Am. Chem. Soc.* **2014**, *136*, 1333.
(96) Schurko, R. W.; Hung, I.; Macdonald, C. L. B.; Cowley, A. H. *J. Am. Chem. Soc.* **2002**, *124*, 13204.
(97) Rossini, A. J.; Hung, I.; Johnson, S. A.; Slebodnick, C.; Mensch, M.; Deck, P. A.; Schurko, R. W. *J. Am. Chem. Soc.* **2010**, *132*, 18301.

DOI: 10.1021/jacs.6b00071
J. Am. Chem. Soc. 2016, 138, 3831−3843